POLITECNICO MILANO 1863

DEIB – Dipartimento di Elettronica, Informazione e Bioingegneria
Politecnico di Milano
DAER - Dipartimento di Scienze e Tecnologie Aerospaziali
Politecnico di Milano

– Master thesis –

Use of High-Resolution Numerical Weather Predictions for the Design and Operation of Earth-space Links

Academic year : 2019/2020

Student

Wioland Bastien
Student ID : 915963
School of Industrial and Information Engineering - Space engineering

Supervisor

Luini Lorenzo, Assistant professor, DEIB – Dipartimento di Elettronica, Informazione e Bioingegneria, Politecnico di Milano

Co - Supervisor

Lavagna Michèle, Full Professor in Flight Mechanics, Department of Aerospace Science and Tecnology, Politecnico di Milano

July 8, 2020

Acknowledgments

I would like to express my sincere thanks to Pr. Lorenzo Luini, first for his clarity and dynamism as a professor of Telecommunication Systems, introducing me and stimulating my interest to this subject. I wish to thank him for accepting to supervise me for this thesis, for giving me such a great support and for being always available and understanding in spite of the distance.

I would also like to thank my home university, ENSMA, for giving me the great opportunity of studying abroad at Politecnico di Milano as a double degree student to complete my education in space engineering. In particular I would like to thank Maggy Sourisseau and Aurélie Cotillon for their help and their support regarding my experience in Italy.

Abstract

The increasing use of satellites has led to the saturation of the lower frequency bands (e.g. Ku band). Consequently new technological solutions are investigated so that higher bands (e.g. Ka band, Q band and V band) can be exploited by the next generations of communication systems, giving access to wider bandwidths. However high frequencies suffer more from tropospheric impairments, including absorption and scattering due to rain, clouds and gases.

In this context, this thesis aims at exploring the use of of the high-resolution numerical weather predictions provided by the The Weather Research and Forecasting model (WRF) to predict tropospheric impairments affecting Earth-space links.

Specifically, the work presented in this thesis aims at using these refined high resolution forecasts for the prediction of tropospheric attenuation for Earth-space links at frequencies in the K- and Ka-band. In turn, these outcomes can be used both to design the link (e.g. transmit power) and for its operation, for example by adapting the modulation and coding scheme on the basis of the attenuation predicted in advance. Indeed, the accurate characterization of the troposheric signal attenuation represents a main challenge for the design of new satellite communication systems.

Table of contents

Index of figures

Index of Tables

List of Abbreviated Terms

CDS	Climate Data Store
API	Application Programming Interface
ECMWF	European Centre for Medium-Range Weather Forecasts
ARW	Advanced Research WRF
WPS	WRF Preprocessing System
UTC	Universal Time Coordinated
DSD	Drop Size Distribution
ITU	International Telecommunication Union
LON	Longitude
LAT	Latitude
ALT	Altitude
CCDF	Complementary cumulative Distribution Function

1 Introduction

The operational frequencies of new generations of satellite communication systems are progressively shifting to higher bands, due to the congestion of the lower frequencies associated to the increase in the number of operating satellites, and to take advantage of the wider frequency bandwidths that they provide. However this increase in frequency exposes the communication link to strong tropospheric impairments.

Indeed, Earth-Space links exploit electromagnetics waves that are influenced by the environment across which they propagate. While the impact is relatively limited for systems operating at low frequencies, the impairments due to tropospheric propagation becomes particularly significant for frequencies higher than 10 GHz. First, the presence of gases with high density such as oxygen and water vapour induces the partial absorption of the electromagnetic energy, more intensely around their molecular resonance frequencies. Then the cloud cover affects the signal mainly by partially scattering the electromagnetic waves and by partially absorbing its energy. Finally more sporadic events such as rain have a strong impact on the propagation in terms of attenuation, and can jeopardize the Earth-link communication. The signal attenuation is dependent on the density of the gaseous components and the intensity of the meteorological events, and thus it is time and space dependent. Consequently the attenuation prediction should be performed by using fine meteorological data capable of adequately capturing these meteorological events in space and time.

Current Numerical Weather Prediction (NWP) models provide a reliable solution for the generation of high resolution weather forecasts. In particular their combination with medium resolution atmospheric and climate variables allows the generation of high resolution meteorological data. This thesis investigates the combination of the ERA5 weather dataset provided by ECMWF and the The Weather Research and Forecasting (WRF) model to generate high resolution meteorological data. The ERA5 dataset provides hourly estimates of a large number of atmospheric variables, covering the Earth on a 30km grid and resolving the atmosphere using 137 levels from the surface up to a height of 80km. This resolution is not fine enough to capture the localized and sporadic events such as rain, and the spatial distribution of clouds and gases. Thus in order to optimize the attenuation prediction, the resolution of the ERA5 data is increased by means of WRF model.

A reliable prediction of the signal attenuation is particularly important for the new generations of satellite communication systems since the high impact of the tropospheric impairments has to be taken into account in the design process of the telecommunication link in order to minimize the link interruptions but also during the operational life of the satellite to anticipate and prevent link outages (e.g. by dynamically adapting the modulation and coding scheme to the link state).

The thesis is organized as follows. Chapter 2 briefly presents the foundations of the propagation of electromagnetic waves through the troposphere. Chapter 3 introduces the WRF model and presents the specifications, the parametrization, and the outputs of the model. Chapter 4 presents the ERA5 dataset used for the initialization of the WRF model, the variables contained in the dataset, their resolution and the download process. Chapter 5 deals with the implementation of the WRF outputs for the computation of the tropospheric attenuation. The Earth-Space reference link is introduced, then the setup for the WRF simulation is presented and finally the tropospheric attenuation evaluation process is presented. Chapter 6 synthesizes the outcomes of the simulation and comments the main results.

2 Tropospheric effects

Electromagnetic radiation is efficiently used for communications and the transmission of information between ground stations and satellites. However the propagation of elecromagnetic waves can be strongly influenced by the presence of hydrometeors (rain, snow, hail, fog...) and the composition of the atmosphere. Above 10 GHz, these effects are mainly bounded to the troposphere and can be fully neglected above an altitude of 30km.

The most relevant effects on the propagation of electromagnetic waves are:

- attenuation
- interferences due to scattering
- depolarization
- scintillations

All of the effects listed above will tend to decrease the amount of power carried by the wave in the receiver's direction, save for scintillations which induce a fast fluctuations of the received signal. If the power received is too attenuated the signal to noise ratio can drop below the requirements and compromise the communication.

2.1 Gaseous attenuation

In the 1-1000 GHz range, gaseous attenuation is primarily caused by the presence of oxygen and water vapour. Indeed, depending on the frequency of the incoming signal, the molecules will absorb part of the energy, especially when the frequency corresponds to the molecular resonance : this phenomenon is very frequency selective. If for low frequency the attenuation is lower than 0.5dB/km, its impact on the signal link becomes higher than 0.5dB/km for frequencies higher than 15 GHz. The specific attenuation of oxygen and water vapour is reported in figure 1 for a particular pressure, temperature and humidity condition.

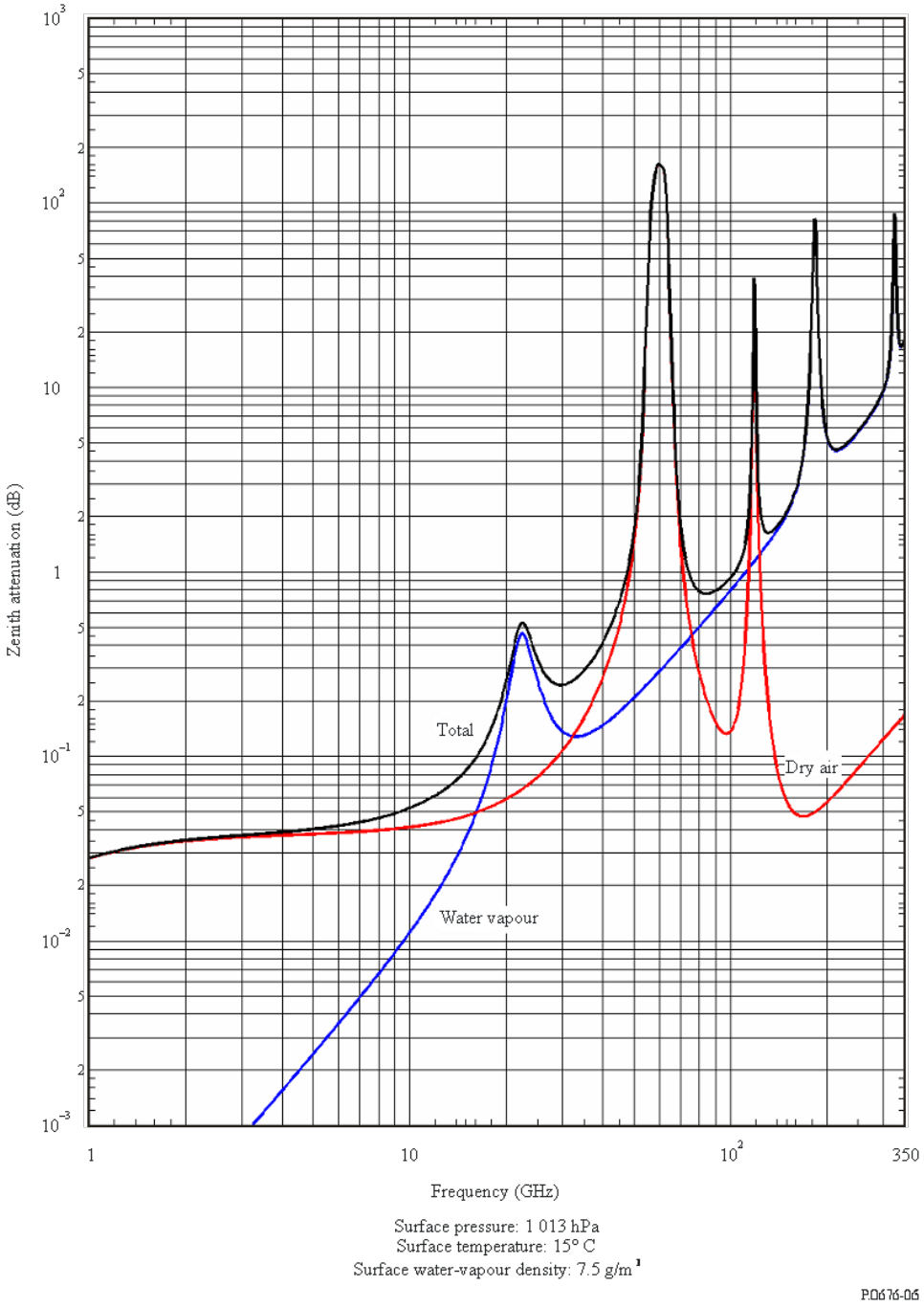

Figure 1: Total, dry air and water-vapour zenith attenuation at sea level [1]

The prediction of the attenuation requires a good knowledge of the meteorological conditions. Indeed it is dependent on the pressure, temperature and the water vapour density. These parameters are space and time dependent, and are consequently changing along the slant path of the link.

In this work, the attenuation is computed following the ITU-R P.676-10 [1] recommendation. The method proposed by this reference is based on a line-by-line method. It is valid in the 1-1000 GHz frequency range and is limited to the oxygen and water vapour attenuation. It implies the computation of the specific attenuation from the oxygen for dry air and the specific attenuation

from water vapour separately. Therefore the total gaseous attenuation can be expressed as :

$$\gamma_{gaseous} = \gamma_{water\ vapour} + \gamma_{oxygen} \tag{1}$$

Figure 2 summarizes the input variables required for the computation of the gaseous specific attenuation.

Figure 2: Inputs required for the gaseous attenuation computation

2.2 Rain attenuation

When an electromagnetic wave impinges on a water drop, two main phenomena occur :

- part of the energy is absorbed and tends to heat up the drop
- part of the incident energy is scattered in all directions

This phenomenon can be mathematically modelled considering that all the water particles are small antennas with an extinction section C_{ext}. Therefore the energy removed by the rain drop from the signal can be written as :

$$P_{lost} = C_{ext} * S_i \tag{2}$$

with S_i the incident power density. P_{lost} can be divided between the contribution of absorption and scattering :

$$P_{lost} = P_{abs} + P_{sc} = C_{abs} * S_i + C_{sc} * S_i \tag{3}$$

The evaluation of the extinction section is a complex problem since it depends on several different parameters :

- particle shape
- particle dimension
- particle dielectric constant (water temperature)
- wave frequency
- wave polarization
- incident angle

However, rain can be modelled using a statistical approach. Indeed rain is composed of a large population of particles that present different properties in term of size and shape. This population is generally modelled by the Drop Size Distribution (DSD), called $N(D)$. This parameter defines the number of particles per cubic meter and with diameter D $\in [D - dD/2, D+dD/2]$, with dD being a small variation in the diameter. Since the drop distribution is highly variable from event to event, it is very difficult to have an accurate estimation. However several empirical laws can be used and depend mainly on the rain rate.

The attenuation is computed following the ITU-R P.838-3 recommendation. The method is highly dependant on the meteorological input data, especially the rain rate, the rain water density, the temperature, the pressure and the air density.
The specific rain attenuation γ_R is derived using the power law relationship :

$$\gamma_R = kR^{\alpha} \tag{4}$$

where R is the rain rate in mm/h, k and α are frequency dependant coefficients. This procedure allows for the introduction of linear and circular polarization.

$$log_{10}k = \sum_{j=1}^{4} \left(a_j exp\left[-\left(\frac{log_{10}f - b_j}{c_j} \right)^2 \right] \right) + m_k log_{10}f + c_k \tag{5}$$

$$\alpha = \sum_{j=1}^{5} \left(a_j exp\left[-\left(\frac{log_{10}f - b_j}{c_j} \right)^2 \right] \right) + m_\alpha log_{10}f + c_\alpha \tag{6}$$

Where f is the frequency of the signal in GHz and k and α can be vertical or horizontal polarization.

The additional coefficients a, b, c and m are reported in the following tables : k_H in Table 1 ,k_V in Table 2,α_H in Table 3 and α_V in Table 4. H stands for horizontal polarization and V for vertical polarization.

Table 1: Coefficients for k_H

j	a_j	b_j	c_j	m_k	c_k
1	-5.33980	-0.10008	1.13098	-0.18961	0.71147
2	-0.35351	1.26970	0.45400		
3	-0.23789	0.86036	0.15354		
4	-0.94158	0.64552	0.16817		

Table 2: Coefficients for k_V

j	a_j	b_j	c_j	m_k	c_k
1	-3.80595	0.56934	0.81061	-0.16398	0.63297
2	-3.44965	-0.22911	0.51059		
3	-0.39902	0.73042	0.11899		
4	0.50167	1.07319	0.27195		

Table 3: Coefficients for α_H

j	a_j	b_j	c_j	m_α	c_α
1	-0.14318	1.82442	-0.55187	0.67849	-1.95537
2	0.29591	0.77564	0.19822		
3	0.32177	0.63773	0.13164		
4	-5.37610	-0.96230	1.47828		
5	16.1721	-3.29980	3.43990		

Table 4: Coefficients for α_V

j	a_j	b_j	c_j	m_α	c_α
1	-0.07771	2.33840	-0.76284	-0.053739	0.83433
2	0.56727	0.95545	0.54039		
3	-0.20238	1.14520	0.26809		
4	-48.2991	0.791669	0.116226		
5	48.5833	0.791459	0.16479		

The coefficients k and α for linear and circular polarization can be derived from the equations 5 and 6 using the following expressions :

$$k = \frac{k_H + k_V + (k_H - k_V)cos^2(\theta)cos(2\tau)}{2} \tag{7}$$

$$k = \frac{k_H\alpha_H + k_V\alpha_V + (k_H\alpha_H - k_V\alpha_V)cos^2(\theta)cos(2\tau)}{2k} \tag{8}$$

where θ is the path elevation angle and τ is the polarization tilt angle relative to the horizontal.

The values for k_H, k_V, α_H and α_V can be found tabulated as a function of the frequency in the ITU-R P.838-3 documentation. [2]

Figure 3 summarizes the input variables required for the computation of the rain specific attenuation.

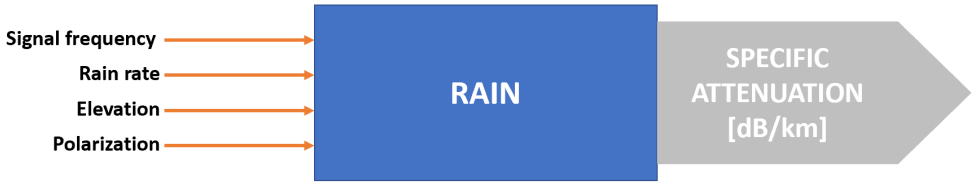

Figure 3: Inputs required for the rain attenuation computation

2.3 Cloud and fog attenuation

The attenuation mechanism is very similar to the rain attenuation. However the size of the water particles in clouds and fog is significantly smaller and homogeneous compared to rain events. This leads to a better accuracy in the attenuation estimation since it does not depend on the size distribution. In addition, due to their small size, clouds and fogs are only significantly attenuating signals with a carrier frequency higher than 30GHz.

Their attenuation is computed according to the ITU-R P.840-8 recommendation [3].

While the size of the water droplets is less than 0.01 cm, the Rayleigh approximation underpinning the method included in [3] is valid for frequencies below 200 GHz.

The specific attenuation can be expressed as :

$$\gamma_c = K_l M \tag{9}$$

where γ_c is the specific attenuation due to fog and cloud in dB/km, K_l is the specific attenuation coefficient in $(dB/km)/(g/m^3)$ and M is the liquid water density in the cloud or fog in g/m^3.

The specific attenuation coefficient K_l can be computed using a mathematical model based on Rayleigh scattering, which uses a double-Debye model for the dielectric permittivity $\epsilon(f)$ of water.

$$K_l = \frac{0.819 f}{\epsilon''(1+\nu^2)} \qquad (dB/km)/(g/m^3) \tag{10}$$

With f being the signal frequency. Then ν can be expressed as a function of the complex dielectric permittivity of water :

$$\nu = \frac{2+\epsilon'}{\epsilon''} \tag{11}$$

The complex dielectric permittivity of water is :

$$\epsilon''(f) = \frac{f(\epsilon_0 - \epsilon_1)}{f_p[1+\left(\frac{f}{f_p}\right)^2]} + \frac{f(\epsilon_1 - \epsilon_2)}{f_s[1+\left(\frac{f}{f_s}\right)^2]} \tag{12}$$

$$\epsilon'(f) = \frac{\epsilon_0 - \epsilon_1}{1 + \left(\frac{f}{f_p}\right)^2} + \frac{\epsilon_1 - \epsilon_2}{1 + \left(\frac{f}{f_s}\right)^2} + \epsilon_2 \tag{13}$$

Where :

$$\epsilon_0 = 77.66 + 103.3(\theta - 1) \tag{14}$$

$$\epsilon_1 = 0.0671\epsilon_0 \tag{15}$$

$$\epsilon_2 = 3.5 \tag{16}$$

$$\theta = 300/T \tag{17}$$

and T is the temperature in Kelvin.

The principal and secondary relaxation frequencies depend on the temperature and are given by :

$$f_p = 20.20 - 146(\theta - 1) + 316(\theta - 1)^2 \qquad GHz \tag{18}$$

$$f_s = 39.8 f_p \qquad GHz \tag{19}$$

Figure 4 summarizes the input variables required for the computation of the specific attenuation due to fog and clouds.

Figure 4: Inputs required for the fog and cloud attenuation computation

3 The Weather Research and Forecasting model

3.1 Introduction

The Weather Research and Forecasting (WRF) Model is a mesoscale numerical weather prediction system designed for both atmospheric research and operational forecasting applications. This model has the advantage to be very versatile in term of spatial resolution and is used for a wide range of meteorological applications across scales from tens of meters to thousands of kilometers. This model has been created in the 1990's thanks to a collaborative partnership of the National Center for Atmospheric Research (NCAR), the National Oceanic and Atmospheric Administration (represented by the National Centers for Environmental Prediction (NCEP) and the Earth System Research Laboratory), the U.S. Air Force, the Naval Research Laboratory, the University of Oklahoma, and the Federal Aviation Administration (FAA).

The model provides simulations both from idealized cases or real atmospheric data. The model is divided in two dynamical solvers, the Advanced Research WRF (ARW) and the Nonhydrostatic Mesoscale Model (NMM). In this thesis, the Advanced Research WRF is used. This model has been under development since 2011, and provides a state-of-the-art atmospheric simulation system. The equation set for ARW is fully compressible, Eulerian and nonhydrostatic. The time integration scheme in the model is based on the third-order Runge-Kutta scheme, and the spatial discretization employs 2nd to 6th order schemes. [4]

The ARW can be divided in multiple subsytems. Two of them are used in this thesis :

- WRF Preprocessing System (WPS) : this module is used primarily for real-data simulations, it preprocesses the input atmospheric data and makes them compatible for the simulation. In addition it creates all the context and the structure needed to run the simulation. The main functions provided by WPS are :

  (i) the definition of the simulation domains

  (ii) the interpolation of terrestrial data (such as terrain, land use, and soil types) to the simulation domain

  (iii) the degribbing and interpolation of the meteorological data from another model to the simulation domain

- WRF model : it contains the key component of the modeling system, the ARW solver. It is composed of several initialization programs for idealized and real-data simulations, along with the numerical integration program.

The program flow for the computation of real cases is presented in figure 5.

In this thesis the model is used to improve the spatial and time resolution of meteorological data in order to reach the resolution required for a proper estimation of the signal attenuation through the atmosphere.

Figure 5: Program flow for real data cases [5]

3.2 Model specifications

The ARW-WRF is a unix based model, particularly it is well supported on a Linux environment. In order to compile and run the model, the computer should verify the requirements listed in Table 5.

For support in the installation of WRF, the WRF User Page provides a complete a exhaustive tutorial for the installation, compilation and setting of the WRF model. It explains the step by step procedure to follow and includes examples and study cases.[5]

Table 5: Software requirements for the use of WRF model

Software Requirements
Fortran 90 or 95, and a C compiler
perl 5.04 or later
WRF I/O API supports netCDF, pnetCDF, and PHD5
Jasper, libPNG, and Zlib installed for real case simulations using grib2 files

3.3 Key parameters

The WRF-ARW model is highly versatile, leading to a wide choice of options and parameters. This section will focus on the key parameters relevant to run and understand properly the simulations performed in this thesis. A more exhaustive list of the parameters can be found on the WFR User Page website [4] or in the WRF User's Guide [6].

These parameters can be divided in 2 main families : simulation and domain. They define the context and the options of the simulation and have to be chosen carefully. The key parameters are presented in tables 6 and 7. WRF allows the computation of multi-domain simulations. This allows the creation of a nested domain inside the main domain. Nesting of several domains into each other allows for an increase of the spatial resolution. This strategy will be used to reach the ground spatial resolution objective of 1km. This method will be more widely discussed in section 5.2.

Table 6: Key parameters for the simulation

Parameters	Specifications
Starting date	Using the Universal Time Coordinated (UTC)
Ending date	UTC
Input interval time	Time resolution of the input data
Integration time	Time step for the integration. The integration time in seconds is taken as 5 times the spatial resolution in km
History interval	Time resolution of the output data

Table 7: Key parameters for the domain definition

Parameters	Specifications
Number of domain	Defines the number of domain for the simulation
Cell number for each domains	Defined in both North-South and East-West direction
Space resolution for each domain	Defined in both North-South and East-West direction
ID for each domain	
ID of the parent domain	Corresponding to the previous parameter
Position in the parent domain	Position of each child-domain (bottom left corner) inside the parent domain.
Parent grid ratio	Defines the ratio of the spatial grid resolution between the domain and its parent domain. This ratio should be taken between 3 and 5 in order to have coherent results.

3.4 Nested domains

The ARW-WRF model allows for multi-domain simulations, and particularly for imbricated domains. The purpose of this method is to scale down progressively the meshing. Indeed a good practice is to use a grid resolution for the main domain close to the grid resolution of the input data. Then for each child domain a grid ratio between 3 and 5 can be applied. Thus, for three imbricated domains, the grid resolution can be improved up to 25 times with reasonable grid ratios.

In addition the model allows for the use of dynamical domains, for which their position in space can be time dependant. This option can be useful to optimize dynamically the size of the domain and consequently the computational time for the tracking of a non-geostationary satellite for example.

3.5 Outputs

The ARW-WRF model produces Netcdf/Grib output files containing all the meteorological variables. Each variable can depend on four parameters : the latitude, the longitude, the altitude and the time. The size and distribution of these variables are fully driven by the parameters presented in section 3.3 and are consequently chosen by the user. The variables

dependency and dimensions are stored in the header of the output file and can be accessed using the netCDF command 'ncdump -h'.

	ncdump -h wrfout_d<domain>_<date>
Example :	netcdf wrfout_d01_2000-01-24_12:00:00

These data can be read and exploited inside a Matlab environment using the free toolbox NCTOOLBOX [7]. More specifically the function ncgeodataset is used for opening the file inside Matlab and transforms the WRF output file into a Matlab structure.

The list of all the variables available as output of a WRF simulation can be found in the WRF User manual [6]. The set of variables written inside the output files can be chosen by the user. A proper choice of the set of variables can be useful to limit the final size of these output files. The specified set of variables written in the output file can differ from the parent domain to its child domains.

4 WRF input Data

The initialisation of the WRF model for real cases can be performed using large-scale coarse-resolution meteorological data available online. The WRF User Website provides a list of compatible sources [8]. According to the website, the best compromise to have good time and spatial resolution is to use ERA5 reanalysis data. It should be noticed that the NCEP GFS dataset could be a good alternative, having a equivalent spatial resolution but a lower time resolution. The spatial and time resolution for the two datasets are presented in table 8.

Table 8: Spatial and time resolution for input datasets

Dataset	Spatial resolution	Time resolution
ERA5 reanalysis	31km (0.25°)	hourly
NCEP GFS	0.25°	3-hourly (for first 240 hrs) then 12-hourly (hrs 240-384)

The ERA5 dataset is selected for the simulations. The ARW-WRF model allows the direct use of this dataset, the compatibility is achieved during the preprocessing phase (WPS) using the integrated Vtable corresponding to the ERA5 dataset.

4.1 ERA5 dataset

ERA5 is the fifth generation of ECMWF atmospheric reanalysis of the global climate, covering the period from January 1979 to present. It is produced by the Copernicus Climate Change Service (C3S) at ECMWF.

ERA5 provides hourly estimates of a large number of atmospheric, land and oceanic climate variables. The data cover the Earth on a 30km grid and resolve the atmosphere using 137 levels from the surface up to a height of 80km.

4.2 Requirements

Any user can access the family of ERA5 data-sets via the Climate Data Store (CDS) infrastructure. The access and download is free and not restricted in time and size. The user should be registered on the CDS website. Thanks to the CDS account, the user can download the data using the CDS download web form interface or get his user number and key in order to use API requests.
This second method is implemented in this thesis for the download of the data since it allows more download options. It is a Python based method. It is highly recommended to use the last version of the package that can be found on the Python Package Index (PyPi) website [9].

4.3 Download through API requests

The requests for the data are written in Python. This method contains a wide range of options for the download of the data. Two types of data can be used : pressure levels and model levels. The difference between these two sets is the discretization of the altitude.

For the pressure levels, the altitude is modelled with 37 levels. They correspond to a discretization of the altitude in term of potential pressure. Consequently the altitude corresponding to each level varies in time and space and has to be computed during the post processing of the

data.
On the other hand the model levels consist of 1 to 137 different levels.

However the access to this set is slower. While the pressure levels ERA5 reanalysis data are stored on CDS disks and can be access quickly in some seconds, the model levels dataset belongs to the ERA5-complete reanalysis set and is not stored online on the CDS disk. Due to the vast volume of these datasets (currently about 6 petabyte) these are not stored on spinning disks, but reside in the ECMWF's MARS tape archive instead. Access to this data is in general much slower, approximately several hours. Table 9 summarizes the main differences between pressure and model levels. Model levels data are selected for this thesis.

Table 9: Differences between pressure and model levels

	Number of levels	**Access**
Pressure levels	37	Fast
Model levels	137	Slow

Figure 6 displays several examples of the data obtained from the ERA5 dataset.

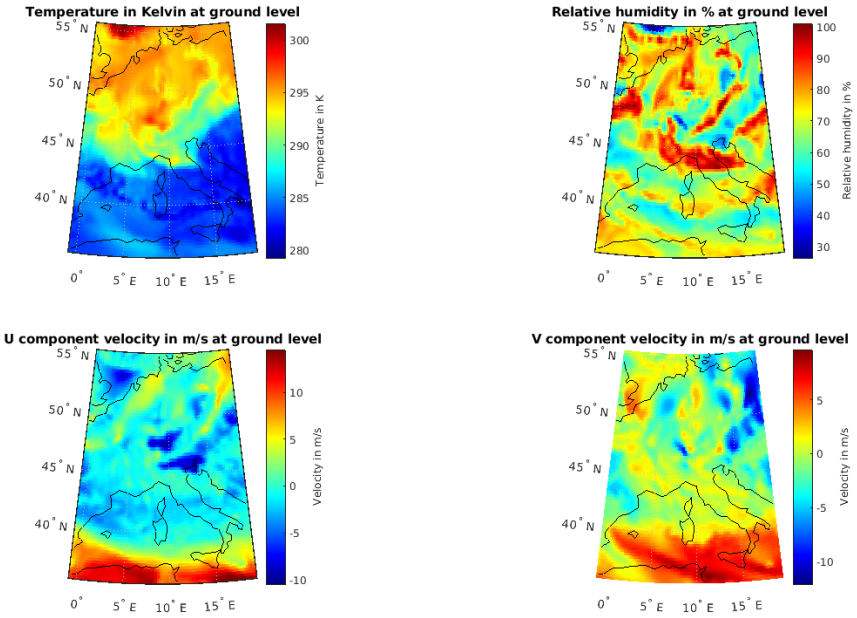

Figure 6: Example of meteorological variables obtained from the ERA5 dataset

5 Study case

This section presents an overview of the code implementation to predict the tropospheric attenuation along Earth-space links. Firstly, the Earth-space link used as reference for this thesis is presented in section 5.1. The whole thesis aims at predicting the tropospheric attenuation for this particular configuration that represents an experimental set-up between a ground station and an operating satellite. Modelling a real experimental set-up is advantageous in terms of model validation. Indeed, the numerical predictions obtained from the WRF simulation can be compared with measurements and finally the performance of the prediction can be evaluated.

Then the parameterization of the WRF simulation is presented in section 5.2 and in particular the definition of the simulation domains in section 5.2.2.

Section 5.4 explains the guideline followed during the code implementation. Section 5.4.2 focuses on the computation of the tropospheric attenuation from the WRF output variables, based on the implementation of the process presented in section 2.

5.1 Reference Earth-space link

The Earth-space link considered in this thesis represents an experimental set-up composed of a ground station in Italy and a operational geosynchronous satellite. The coordinate information for the satellite and the ground station can be found in table 10 and 11.

Table 10: Ground station coordinates

Latitude	**Longitude**	**Altitude**
45.48° N	9.23° E	137 m a.m.s.l.

Table 11: Satellite orbit information

Satellite	**Orbit**	**Coordinates**
Alphasat	Geosynchronous	25° E

Alphasat is the largest European telecom satellite ever built. It has been launched in 2013 for a 15 years mission and carries the Aldo Paraboni Q/V Communications and Propagation payload. It explores new frequencies for future telecommunication applications. One of its main objectives is the estimation of how the Earth's atmosphere affects communications in the Ka-band and Q-band. It uses two continuous-wave beacons at 19.701 GHz and 39.402 GHz (see figure 7). This mission is particularly valuable for the development of propagation models for future Q-, V- and W- band systems and non-geostationary Ka-band systems.

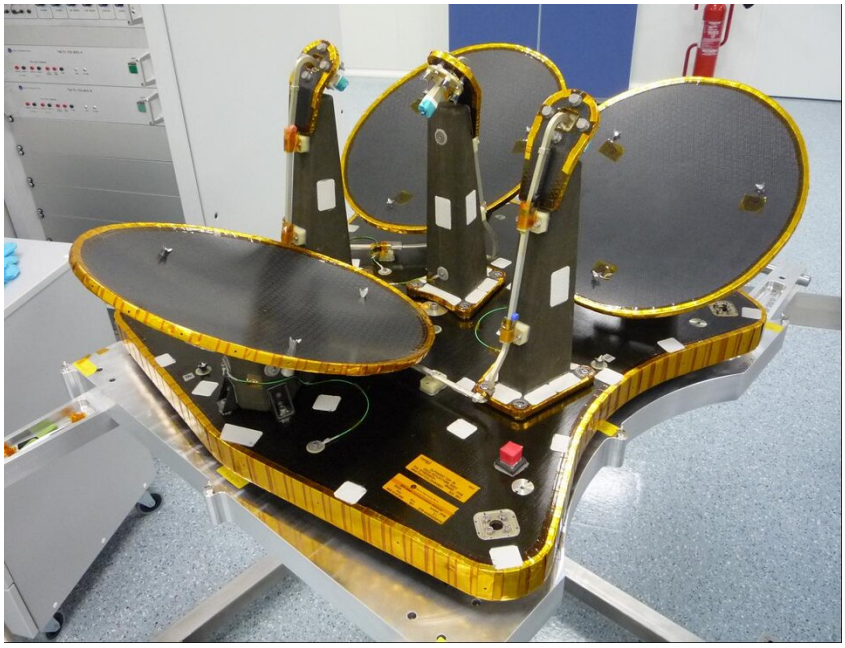

Figure 7: Aldo Paraboni Q/V Band Payload - Picture taken from the ESA website

A receiving station is installed on the rooftop of a building in the main campus of Politecnico di Milano in Milan, Italy. The experimental equipment, developed and owned by NASA Glenn Research Center (GRC), includes two receivers recording the beacon power at 8 samples/second. The diameter of the receiving antennas is 1.2 m (Ka band) and 0.6 m (Q band), respectively, and both receivers are equipped with step motors to track the Alphasat satellite, whose orbital plane has a variable inclination angle, slowly drifting up to 3° (the average link elevation angle in Milan is 35.6°). In addition, collocated with the beacon receivers are:

- weather station, measuring pressure P, temperature T and relative humidity RH at ground level.
- tipping bucket to measure the precipitation rate R.
- A Thies Clima disdrometer operating by means of an infrared laser diode, which generates a 785 nm beam over an area of 4560 mm^2. The observed falling particles (rain, snow flakes, hail, ...) are classified into spectra of 22 diameter bins from 0.125 mm to 8 mm and 20 velocity bins from 0 to 10 m/s with non-uniform bin widths.
- A multi-channel microwave radiometer (23.84, 31.4, 72.5 and 82.5 GHz), MWR, pointed along the path to the Alphasat satellite to derive the integrated liquid water content and the integrated water vapor content, from which the tropospheric attenuation, in non rainy conditions, can be in turn calculated.

For simplicity, the attitude of the spacecraft and its orbit are assumed to be perfect. Thus the geosynchronous satellite is seen at a constant position in the sky by the ground station. Since the relative positions do not change, the link between them in geodetic latitude, longitude and altitude coordinates is constant with time. Thus the domain required for the WRF simulation is constant from a ground point of view. The variations in the signal attenuation are only resulting from the changes in the atmosphere and not from any movement of the spacecraft. Thus, it allows for a better validation of the link attenuation estimated by means of the WRF

outputs. Nevertheless the simulation could also be performed for a non synchronous satellite considering a moving domain in WRF. The use of a moving domain allows for an optimisation of the size domain and consequently optimizes the computational time.

Due to the high computational time required by WRF and the post processing of the data, this thesis focuses on a two-day simulation, from the 30th of September at 00:00:00 to the 2nd Of October 2018 at 00:00:00. In addition, the simulation conducted focuses on the two operating frequencies of the Aldo Paraboni payload : 19.7 and 39.4 GHz.

5.2 Settings for the WRF simulation

5.2.1 Overview of the simulation

The simulation aims at improving the spatial and time resolutions using the ARW-WRF model of the meteorological input data provided as input to the ARW-WRF model. The data available from the Era5 dataset has a maximal resolution of 0.25° in longitude and latitude, which corresponds approximately to 30 km at mid-latitudes. The objective is to scale down this value to 1 km. To keep reasonable grid ratios between the domains, the resolution is improved two times by a ratio of 5.

The initial time interval is 1 hour. The objective is to obtain a new discretization every minute in order to meet the recommendation from the ITU-R5.4.2. However this second constraint is not limiting. Indeed for computational issues, mostly integration stability, the space (ΔX) and time (ΔT) resolutions should verify the following constraint :

$$\Delta T[sec] = 5 \cdot \Delta X[km] \tag{20}$$

This leads to an integration time of around 5 seconds, consequently much lower than the target of 1 minute. However for storage considerations, the output data will be written and saved in the output file only every minute.

The main characteristics of the simulation are summarized in figure 8 while the program flow is presented in figure 9.

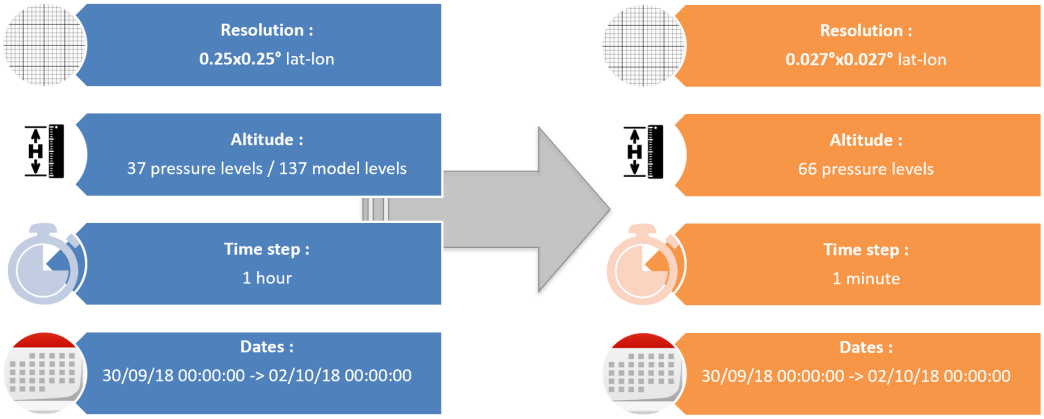

Figure 8: From input to output characteristics

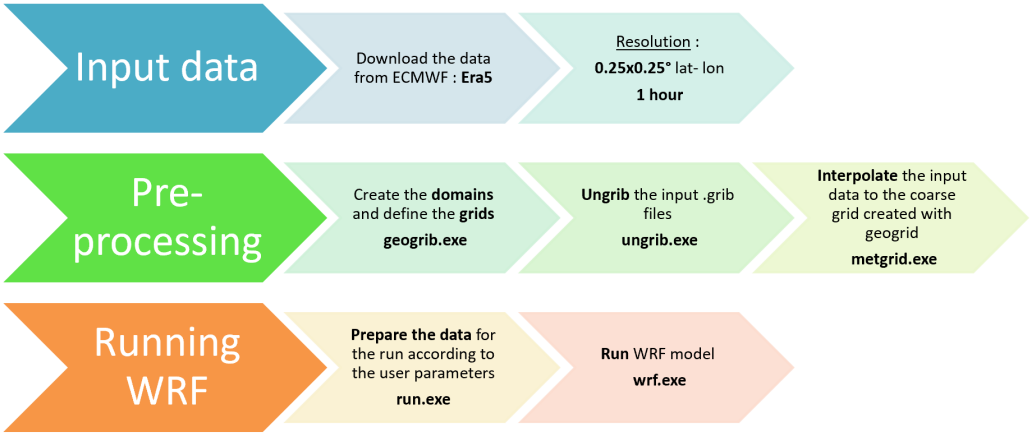

Figure 9: Simulation architecture

5.2.2 Domains definition

The domains used for the WRF simulation depend on the relative position of the ground station and the satellite. To reach the grid resolution close to 1 km, 3 nested domains are used with a relative grid ratio of 5. Figure 10 presents schematically the definition of the domains.

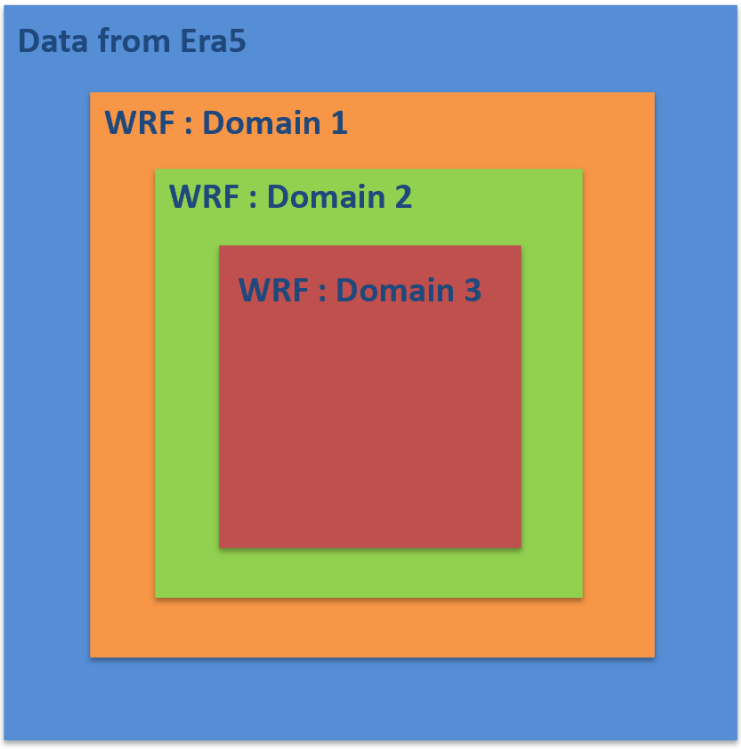

Figure 10: Nested domains

In order to obtain reliable results, the domain definition has to be performed properly following two main rules [10] :

- the grid ratio should be between 3 and 5

- as a rough approximation, about 1/3 of the coarse-grid domain should surround each side of the nested domain.

The impact of the weather on high frequency electromagnetic waves is mainly bounded to the troposphere which extends up to 30 km in height. Thus the domain with high grid resolution, domain 3, has to include only the portion of the troposphere affecting the link. Indeed above 30 km the effect of the atmosphere on the signal attenuation can be fully neglected for a signal frequency higher than 10 GHz.

Table 12 presents the coordinates of the telecommunication link from ground up to 30 km height.

Table 12: Telecommunication link geometry

Altitude	**Latitude**	**Longitude**
Ground	45.48° N	9.23° E
30km	45.1281° N	9.4279° E

The center of the domains is set exactly in the middle between the ground station and the point where the signal leaves the troposphere at 30 km height.

Figures 11, 12 and 13 present the spatial definition of the domains.

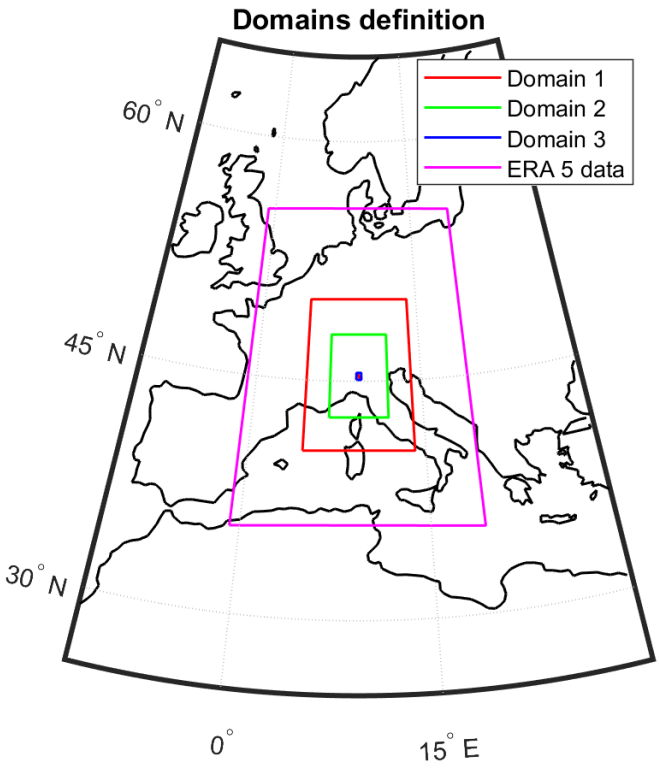

Figure 11: Domain definition

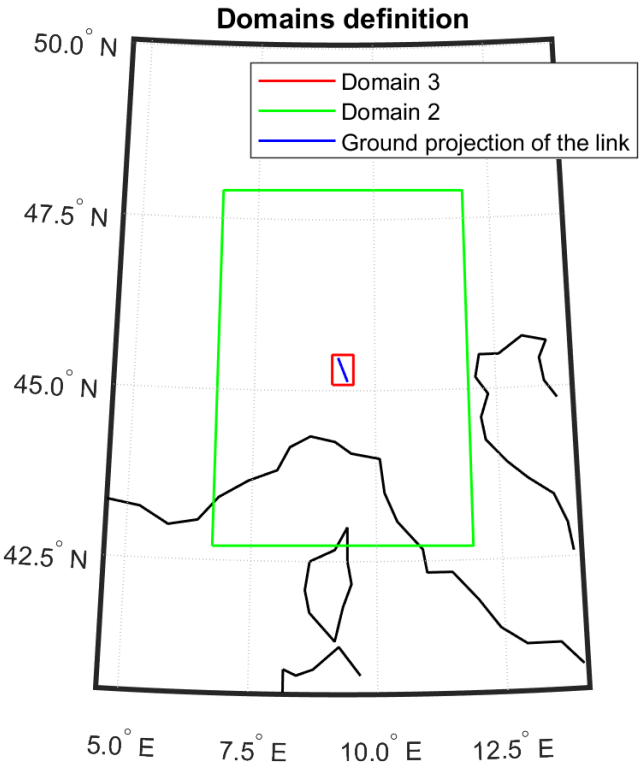

Figure 12: Zoom on domains 2 and 3

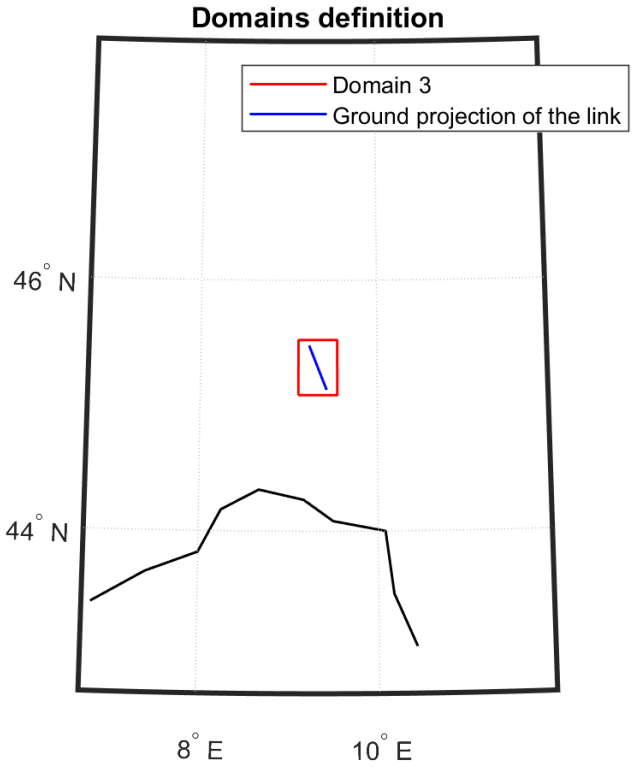

Figure 13: Zoom on domain 3

Figure 14 compares the relative grid dimensions between the domains. The resolution of the first domain matches the resolution of the ERA5 input data. The size of the cells is divided by 5 for each child domain. For comparison the full telecommunication link from ground up to 30 km height fits in two cells with the domain 1 resolution. With the resolution of domain 3, the link fits in a rectangle consisting of 21x37 cells.

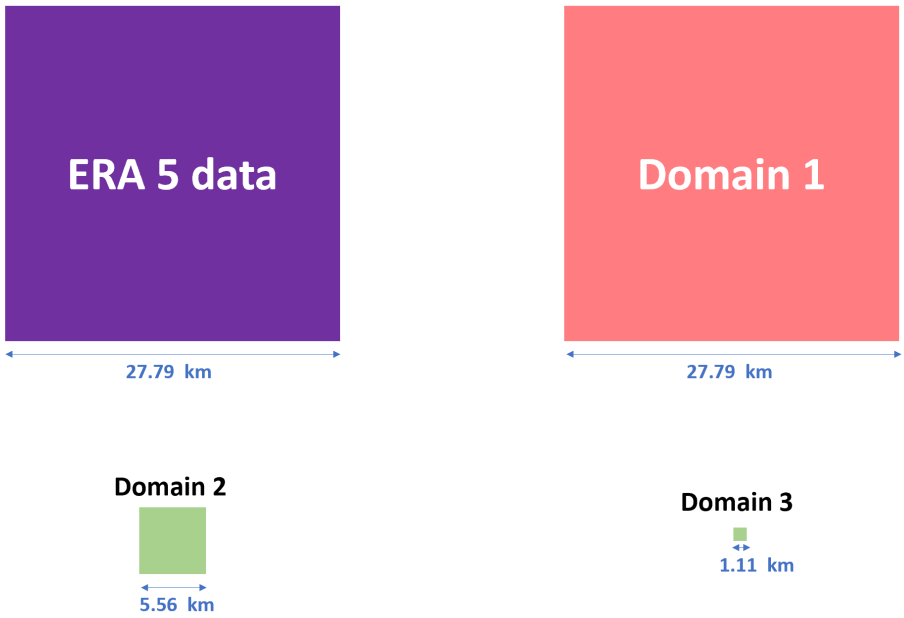

Figure 14: Differences in term of resolution cell

The characteristics of the domains are reported in table 13.

Table 13: Domains characteristics

	Ground resolution in meters	**Grid dimension**	**Latitude range**	**Longitude range**
ERA5 data	27794.37	81x81	[35.48 55.48]°	[359.23 19.23]°
Domain 1	27794.37	40x40	[40.5542 50.0541]°	[4.5785 14.0785]°
Domain 2	5558.874	106x106	[42.7041 47.9041]°	[6.7285 11.9285]°
Domain 3	1111.775	46x46	[45.0841 45.5241]°	[9.1085 9.5485]°

5.3 Raw WRF output data

The temperature, the pressure and the rain water mixing ratio $QRAIN$ at ground level for the 01/10/2018 at 12:00:00 are plotted in figures 15, 16 and 17. Each domain is plotted with its own resolution. A comparison between the resolution of the domain 1, equivalent to the ERA5 data resolution, and the resolution of the nested domain is plotted in figure 18. It can be noted that the improvement of the resolution has a strong impact on the amplitude of the variables. Indeed the events are more localized thanks to the finer resolution and consequently the maximum amplitude increases in the right side plot.

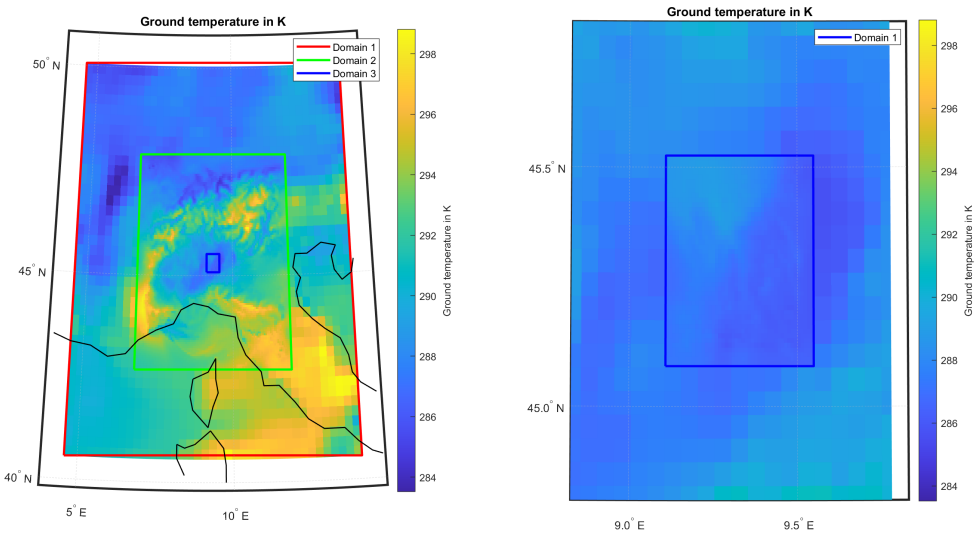

Figure 15: Ground temperature in Kelvin - 01/10/2018 12:00:00

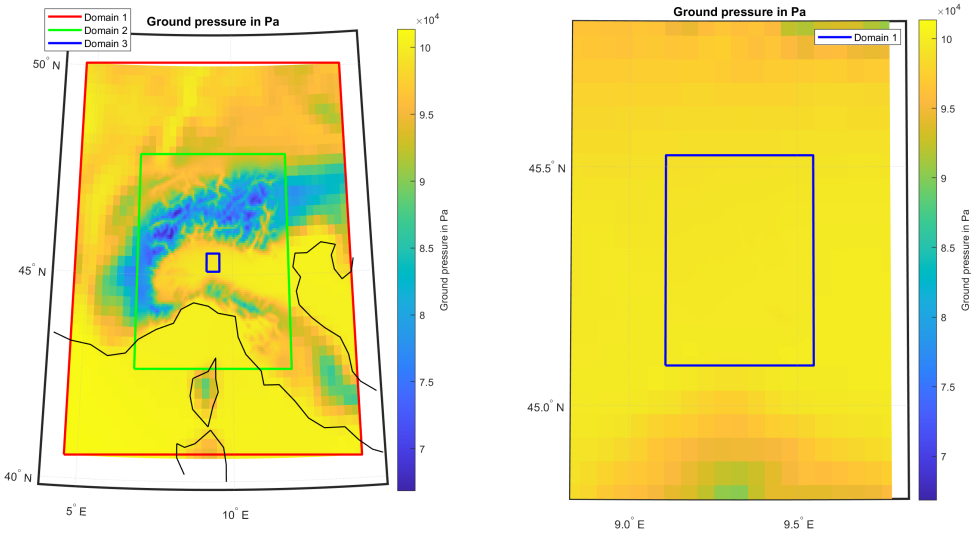

Figure 16: Ground air pressure in Pa - 01/10/2018 12:00:00

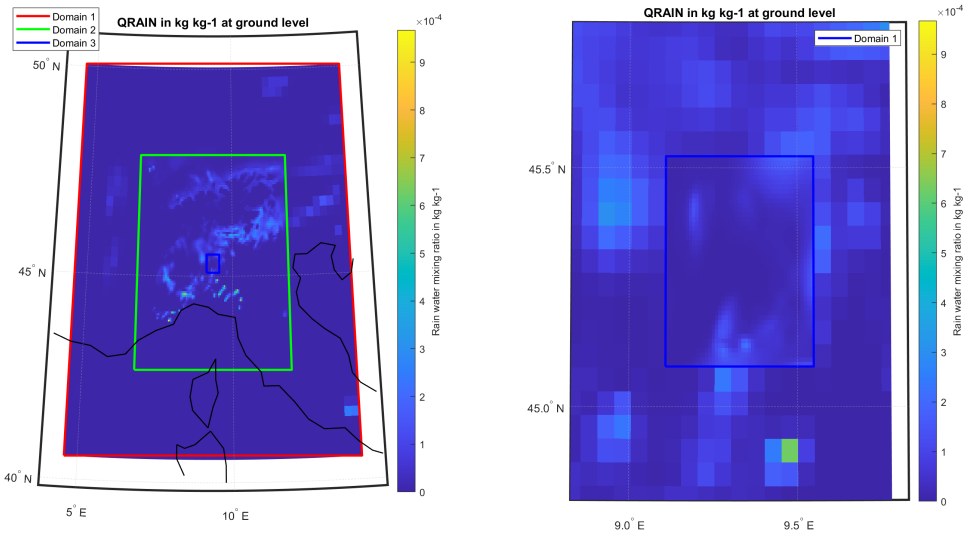

Figure 17: Rain water mixing ratio $QRAIN$ in kg kg^{-1} at ground level - 01/10/2018 12:00:00

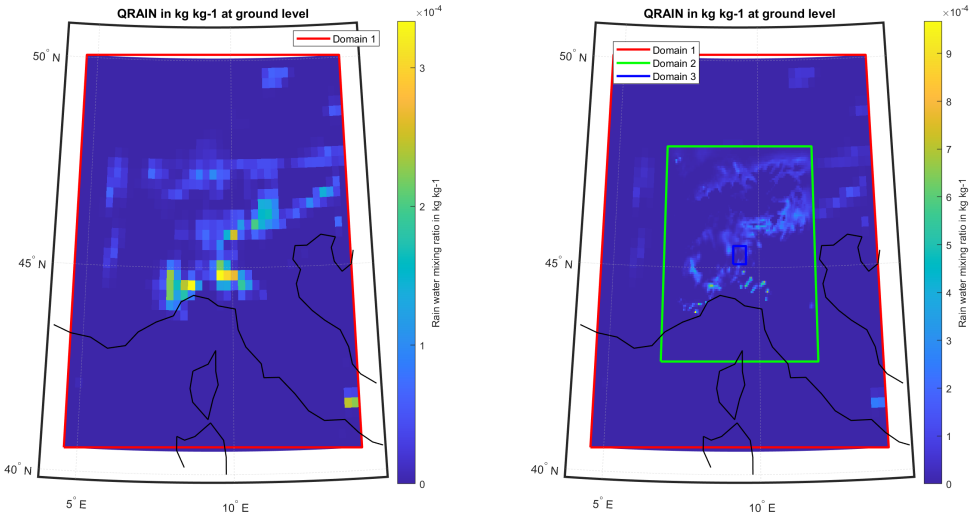

Figure 18: Comparison between raw resolution and nested domain resolution - Rain water mixing ratio $QRAIN$ in kg kg^{-1} at ground level - 01/10/2018 12:00:00

5.4 Post processing

The WRF simulation produces a netcdf output file containing all the meteorological variables requested for the simulation as a function of time, latitude, longitude and altitude. Then the data can be imported into Matlab, specifically in a set of matrices. These matrices contain the meteorological data and can be divided primarily in two families : surface variables and spatial variables. The surface variables are defined at ground level and depend on the longitude, latitude and time. Spatial variables depend also on the altitude. Each pixel of these matrices corresponds to a position in space and time.

$$SURFACE\_DATA(TIME, LATITUDE, LONGITUDE)$$
$$SPATIAL\_DATA(TIME, ALTITUDE, LATITUDE, LONGITUDE)$$

All the variables written by WRF in the output files are reported in table 14

Table 14: Set of variables written by WRF in the output file

Variable Name	Description	Dimensions	Units
PH	Perturbation geopotential	TIME-ALT-LON-LAT	m^2/s^2
PHB	Based-state geopotential	TIME-ALT-LON-LAT	m^2/s^2
T	Perturbation potential temperature theta-T0	TIME-ALT-LON-LAT	K
P	Perturbation pressure	TIME-ALT-LON-LAT	Pa
PB	Base state pressure	TIME-ALT-LON-LAT	Pa
QVAPOUR	Water vapor mixing ratio	TIME-ALT-LON-LAT	$kgkg^{-1}$
QCLOUD	Cloud water mixing ratio	TIME-ALT-LON-LAT	$kgkg^{-1}$
QRAIN	Rain water mixing ratio	TIME-ALT-LON-LAT	$kgkg^{-1}$
SH2O	Soil liquid water	TIME-LON-LAT	m^3m^{-3}
T00	Base state temperature	TIME	K
P00	Base state pressure	TIME	Pa
RAINC	Accumulated total cumulus precipitation	TIME-LON-LAT	mm
RAINSH	Accumulated shallow precipitation	TIME-LON-LAT	mm
RAINNC	Accumulated total grid precipitation	TIME-LON-LAT	mm
XLAT	Latitude, South is negative	TIME-LON-LAT	$^\circ\ North$
XLONG	Longitude, West is negative	TIME-LON-LAT	$^\circ\ East$
z	Synthetized altitude index	ALT	

The values for the time, longitude and latitude are stored in specific matrices. They connect the position of the pixels inside the spatial and surface matrices with their actual position in space and time.

In order to characterize the tropospheric effects affecting the link, these data have to be converted into attenuation. However the transformation of the full set of data into attenuation is not required since the signal will only cross a small part of the voxels. Thus the strategy implemented in this thesis was to identify voxels of the 4D matrices crossed by the links and, afterwards, to compute only the attenuation for these voxels. The implementation of this strategy is exhaustively explained in section 5.4.1.

5.4.1 Slant path identification

For computation efficiency, only the attenuation associated to the voxels crossed by the link are computed.
The link is firstly discretized for every kilometer and the latitude and longitude of each point in the geographic coordinate system is converted into its position in the 4D output matrices of the WRF simulation. This discretization is performed up to the altitude of 30km that represents the upper limit of the simulation. The discretization has been chosen to be smaller than the actual grid resolution of the simulation in order to fully take advantage of the fine resolution. In addition the value is taken only slightly inferior for computational efficiency. Since the spatial resolution is constant with time, the identification of the pixels related to the slant path in term of longitude and latitude can be preformed only once and will be constant for the whole simulation.

For simplicity, the position of the ground station and the spacecraft in lon-lat coordinates can be converted into a new system of variables containing the position of the ground station, the elevation and azimuth of the link. This new representation presents two main advantages :

- easier computation of the slant path for a given altitude
- the elevation is a piece of information required for the computation of the rain attenuation. Indeed since the rain drops are not perfectly spherical due to their acceleration and external aerodynamics forces, the incidence angle ($\simeq$ elevation) of the incoming electromagnetic wave will have an impact on the resulting attenuation.

Figure 19 summarizes the change of variables. The coordinates in this new system are presented in table 15

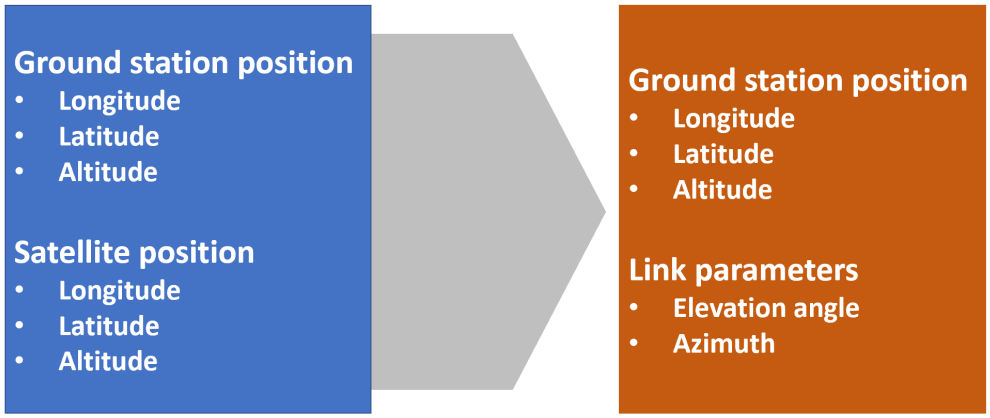

Figure 19: New coordinate system for the link

Table 15: New reference system

Variable	Value	Units
GS latitude	$45.48°N$	degree
GS longitude	$9.23°E$	degree
GS altitude	137	m.a.m.s.l.
Elevation angle	35.3791	degree
Azimuth	158.3781	degree

Figure 20 presents the process for the identification of the voxels indexes in the 4D output matrices. The figure takes the longitude as example. The input is the longitude in degree of the link along its slant path. This continuous variable is then discretized along the slant path, providing the curve on the left side of figure 20. Then for every point of the slant path, the longitude is compared with the longitude discretization of the 4D output matrices. The following vector is set :

$$V = |LON_{output} - lon_i \cdot [1\ 1\ 1\ ...\ 1]| \tag{21}$$

with LON_{output} being a vector containing the longitude discretization of the 4D output matrices and lon_i being the longitude of the link at the position i of the slant path. Thus the index of the minimum value of the vector V corresponds to the index in the 4D output matrices of the longitude lon_i. This identification is iterated for all the i along the link and it is also performed for the latitude.

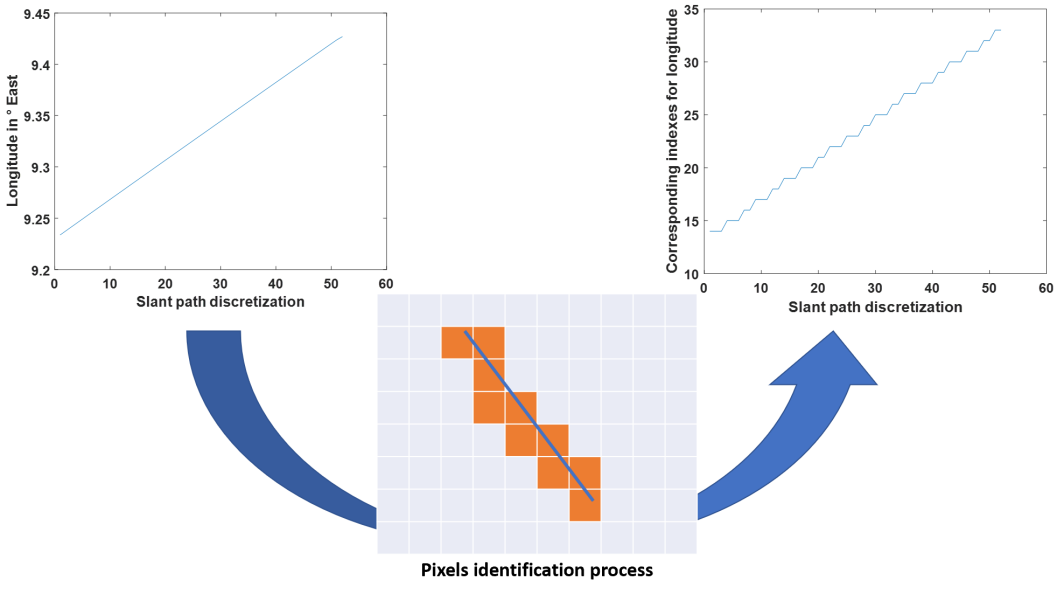

Figure 20: Process of index correspondence for the coordinates

However the identification of the altitude is time dependant. Indeed the output WRF files contain a discretization of the altitude in term of pressure levels. Consequently their corresponding altitude in meters changes with the atmospheric conditions in space and time. The identification of the pixel in altitude should be performed for every time step and position.

The altitude in meters of one pixel of the output file can be easily computed using the perturba-

tion geopotential PH and base-state geopotential PHB, both returned by the WRF simulation.

Therefore the altitude is computed such that :

$$H = \frac{PH + PHB}{g} \tag{22}$$

with H being the altitude in meters, PH and PHB in $\frac{m^2}{s^2}$, and g being the acceleration due to gravity.

$$g = 9.81 \frac{m}{s^2} \tag{23}$$

Finally the slant path is defined for every time step by a list of triplet values corresponding to the longitude index, the latitude index and the altitude index as is shown in figure 21.

Latitude in ° N	45.4732	45.4664	45.4595	45.4527	45.4459	...	45.1404	45.1336	45.1281
Longitude in ° E	9.2338	9.2377	9.2415	9.2454	9.2492	...	9.4201	9.4239	9.4269
Altitude in meters	716	1295	1874	2454	3033	...	29216	29800	30276

Latitude index	40	39	39	38	37	...	7	6	5
Longitude index	14	14	14	15	15	...	32	33	33
Altitude index	7	9	11	13	14	...	94	96	97

Figure 21: Final representation of the slant path

5.4.2 Tropospheric effects prediction

After the discretization of the slant path of the link and the identification of the pixels of interest in the WRF output file, the specific attenuation can be computed. This attenuation is divided into the 4 components presented in section 2 :

- Rain
- Fog and clouds
- Oxygen
- Water vapour

All of these attenuation components are computed separately and then added together to obtain the overall tropospheric attenuation.

The different meteorological variables required for the computation of the link specific attenuation are reported in figures 2, 3 and 4 (section 2).

Rain rate The rain rate can be computed with 2 surface variables from the WRF output file: the accumulated total cumulus precipitation $RAINC$ and the accumulated total grid scale precipitation $RAINNC$. The total accumulated precipitation $RAIN_T$ is the sum of these two variables :

$$RAIN_T = RAINC + RAINNC \tag{24}$$

The rain rate RR can be derived from the last equation by differentiating $RAIN_T$ with time. The rain RR rate is computed as :

$$RR = \frac{(RAIN_T)^{t+1} - (RAIN_T)^t}{dt} \tag{25}$$

with $(RAIN_T)^{t+1}$ being the total accumulated rain at instant $t+1$, $(RAIN_T)^t$ being the total accumulated rain at instant t, and dt being the time step between t and $t+1$.

Rain altitude Rain originates from clouds, where the liquid water droplets that have condensed from atmospheric water vapor becomes heavy enough to fall under gravity. Then the drops fall down to the ground. The rain formation is however a complex process that depends on the atmospheric conditions and on the thickness of the cloud. The rain rate increases progressively from zero up to its maximal value. However, for simplicity, the transient phase of the rain rate is neglected. Thus the rain rate is approximated as constant for all the altitudes from ground to the cloud base [11]. Finally each pixel of the matrix is defined as "rainy" or "not rainy". In order to be marked as a "rainy" pixel, the pixel should have an altitude below the rain altitude.

This altitude is computed from the rain water mixing ratio $QRAIN$. This parameter defines the mass of rain water per unit mass of dry air. It is directly computed during the WRF simulation and is saved in the output files. Thus for strictly positive value of $QRAIN$, the pixel is assumed to be rainy. The rain altitude is thus defined, for any longitude and latitude pixel, and for any time, as the highest altitude with $QRAIN$ strictly positive. This method allows a time and space evaluation of the rain altitude based on the actual meteorological conditions of the atmosphere. Then, for any pixel below the rain altitude, the rain rate can be computed using equation 25.

The method is summarized in figure 22. Starting from the rain water mixing ratio plotted on the left side, the altitude of the rain is computed and then applied to the rain rate.

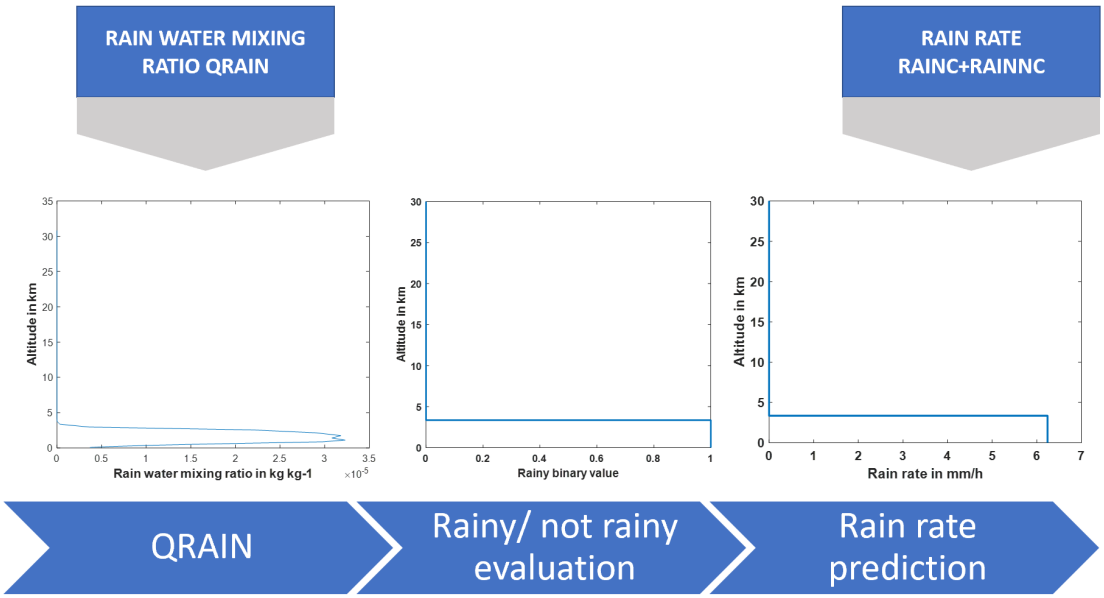

Figure 22: Estimation process of the rain altitude

Air pressure The air pressure is computed as the sum of the based-state pressure PB and the perturbation pressure P.

$$P_a = P + PB \qquad Pa \tag{26}$$

Air temperature The actual air temperature T is computed from the perturbation potential temperature $T0$, output variable of the WRF simulation, and the pressure P in Pa.

$$T = (T0 + 300)\frac{P}{P0}^{\left(\frac{\gamma-1}{\gamma}\right)} \qquad Kelvin \tag{27}$$

with $P0$ being the pressure reference $P0 = 10^5\ Pa$ and γ being the heat capacity ratio for dry air at $20°C$, $\gamma \simeq 1.4$.

Water vapour density The water vapour density M_{wv} can be derived from the water vapor mixing ratio $QVAPOR$, output of the WRF simulation. It can be converted into relative humidity sh :

$$sh = \frac{QVAPOR}{1 + QVAPOR} \tag{28}$$

Then the partial vapour pressure pvp in Pa is computed as:

$$pvp = \frac{sh \cdot P}{0.6225} \qquad Pa \tag{29}$$

Finally the Water vapour density ρ_{wv} is expressed as :

$$\rho_{wv} = \frac{0.0022 \cdot pvp}{T} \qquad kg/m^3 \tag{30}$$

Liquid water density The liquid water density M_l can be derived from the cloud water mixing ratio $QCLOUD$ provided by the WRF simulation and the air density.

The air density can be computed from the usual expression :

$$\rho_{air} = \frac{P}{RT} \qquad kg/m^3 \tag{31}$$

with P being the pressure in Pa, R being the specific gas constant for dry air in J/(kg*K), $R = 287.058$ and T being the air temperature in $Kelvin$. R depends on the temperature. However considering the limited range of air temperature occurring in the troposphere, a constant value of R is a realistic approximation.

Then the liquid water density is :

$$M_l = QCLOUD * \rho_{air} * 1000 \qquad g/m^3 \tag{32}$$

With all the variables derived in this section and the processes presented in section 2, the full set of tropospheric attenuations can be derived.

5.4.3 Full path implementation

The previous section presents how the attenuation can be derived from meteorological data at one position in space and time. In order to generate the full attenuation of the signal in time, these computations have to be extended to the full link and to the whole simulation duration. It is performed by an algorithm based on two imbricated loops, as is shown in figure 23 :

- the outer loop iterates on the different time instants
- the inner loop integrates the specific attenuation along the link. Indeed, as presented in section 5.4.1, its discretisation has led to a series of triplet values of LONGITUDE, LATITUDE and ALTITUDE.

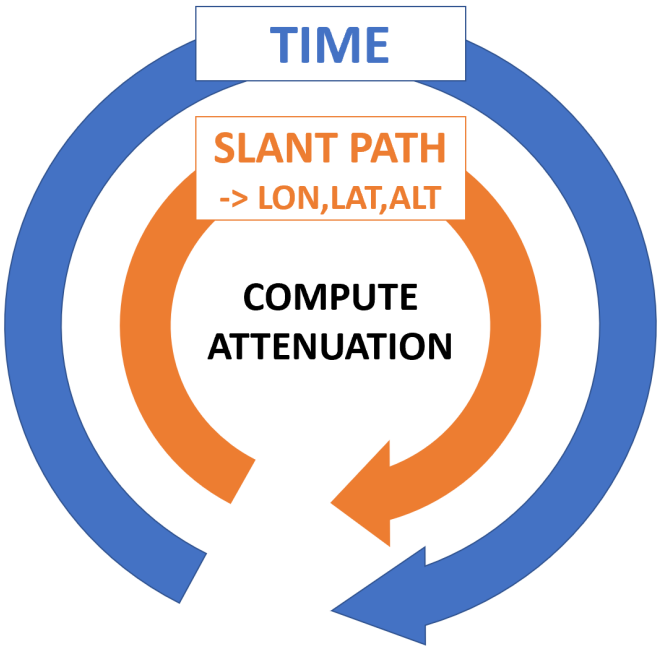

Figure 23: Imbricated loops for the computation of the attenuation

The combination of these two loops leads to a series of quadruplets containing a unique combination of TIME-LONGITUDE-LATITUDE-ALTITUDE. For all of these combinations the specific attenuation for each components are computed and added together to obtain the total attenuation :

$$\gamma_{s,t} = \gamma_{s,r} + \gamma_{s,f} + \gamma_{s,o} + \gamma_{s,wv} \quad dB/km \tag{33}$$

with $\gamma_{s,t}$ being the total specific attenuation, $\gamma_{s,r}$ being the rain specific attenuation, $\gamma_{s,f}$ being the fog and clouds specific attenuation, $\gamma_{s,o}$ being the oxygen specific attenuation and $\gamma_{s,wv}$ being the water vapour specific attenuation.

In dB, the product can be converted into a sum, thus the total attenuation in dB becomes :

$$A = \sum_{i=1}^{N} \gamma_s \quad dB \tag{34}$$

6 Results

6.1 Results for the study case

The results reported in this chapter focus on the two days presented in section 5.2 : the 30th of september and the 1st of october 2018. Such days were selected because of the different meteorological conditions, from clear sky to heavy rain events.

Figures 24 and 25 report the rain rate measured with the disdrometer in Milan.

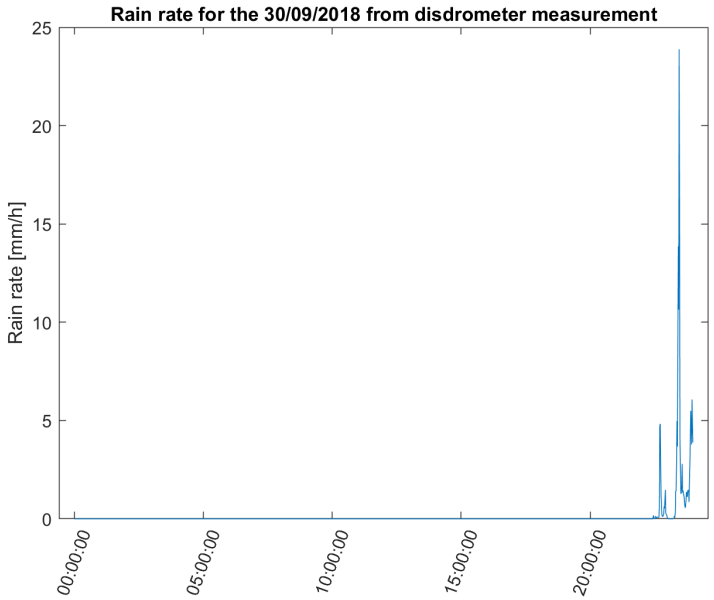

Figure 24: Rain rate measurement with disdrometer - 30/09/2018

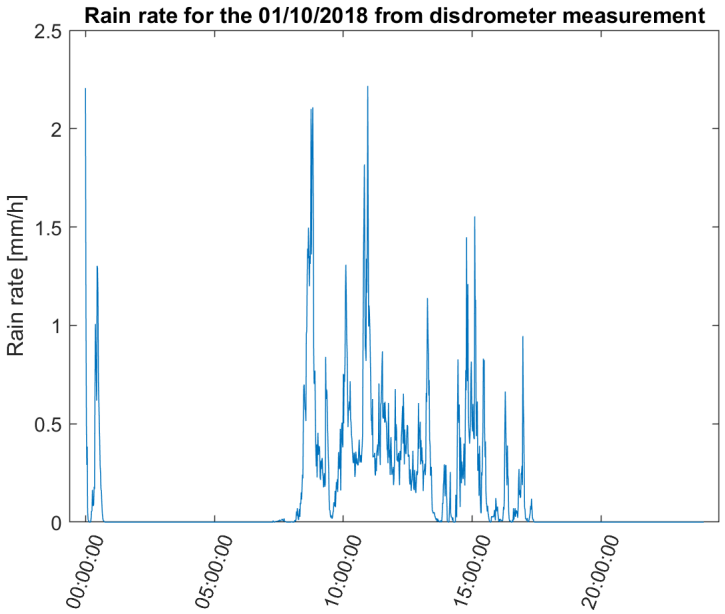

Figure 25: Rain rate measurement with disdrometer - 01/30/2018

Two main rain events can be identified :

- a short and strong one on the 30th September starting around 10pm
- a longer event on the 1st of October but with lower intensity

The rain rate calculated by WRF is reported in figure 26; the data are extracted from the pixel that corresponds to where the ground station is installed.

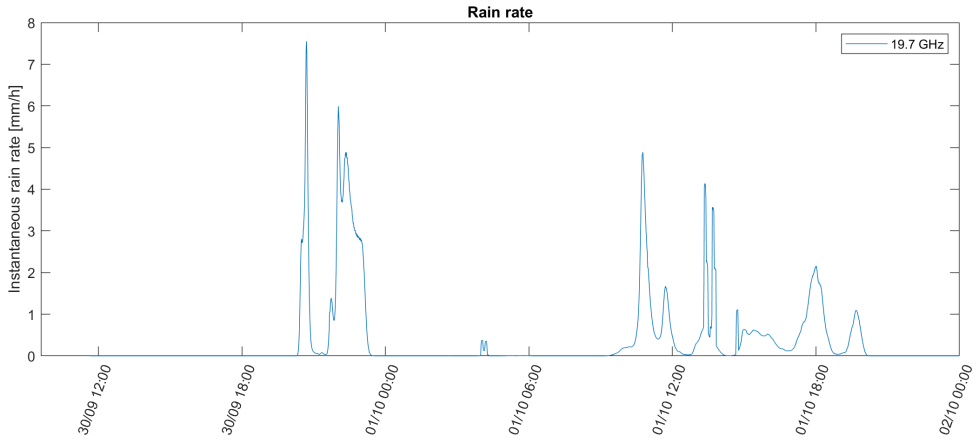

Figure 26: Rain rate in mm/h calculated by WRF

The rain rate measured by the disdrometer and the one computed are compared in figure 27. The accumulated rain amounts are compared in figure 28.

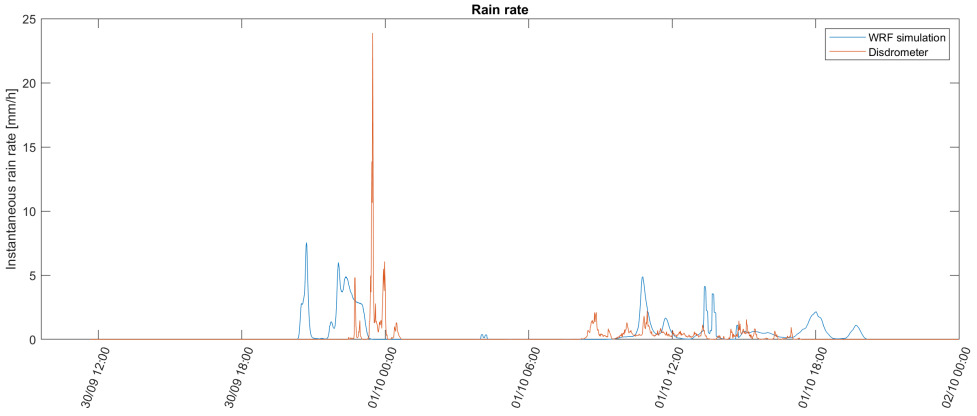

Figure 27: Comparison between measurements and WRF outputs

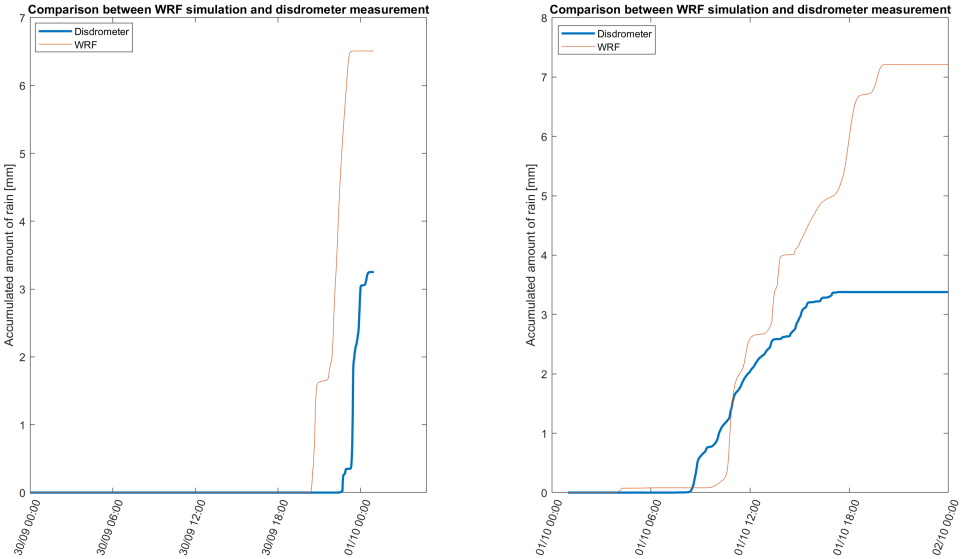

Figure 28: Accumulated rain amounts in mm

The rain rate trends are similar in shape. The similarities are even more visible for the accumulated precipitations in figure 28. However the amplitude of the precipitations is strongly different between the measurement and the prediction. This difference can be explained by the localized nature of the precipitations. Indeed the rain events are limited in space and can undergo strong variations as it can be seen on the figure 17. Figure 29 presents a map of the rain rate around the telecommunication link at ground level and the rain height computed from the WRF simulation. The black line represents projection of the link on the ground. Each pixel represents an area on the ground of approximately $1km^2$. As an example the rainfall on the map covers an area approximately of $25km^2$.

This difference is ascribable to the limited accuracy of the meteorological prediction obtained from the WRF simulation. A sensitivity analysis is performed in section 6.1.2 in order to estimate the influence of an offset in the position of the ground station on the final attenuation obtained.

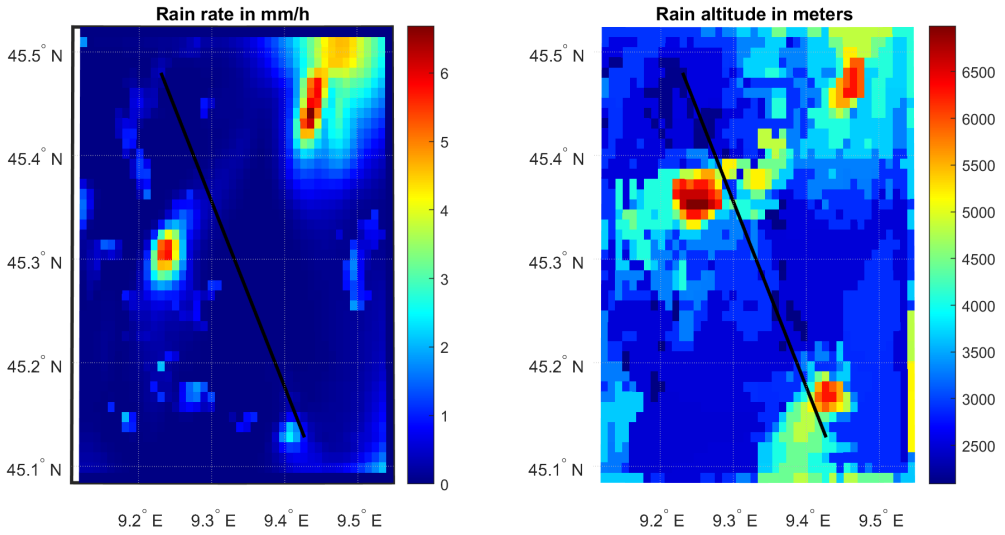

Figure 29: Rain rate at ground level and altitude of the rain for the 01/10/2020 at 1:20pm

Figure 30 presents the total attenuation of the signal at 19.7 GHz, obtained by applying the propagation models outlined in section 5.4.2 above.

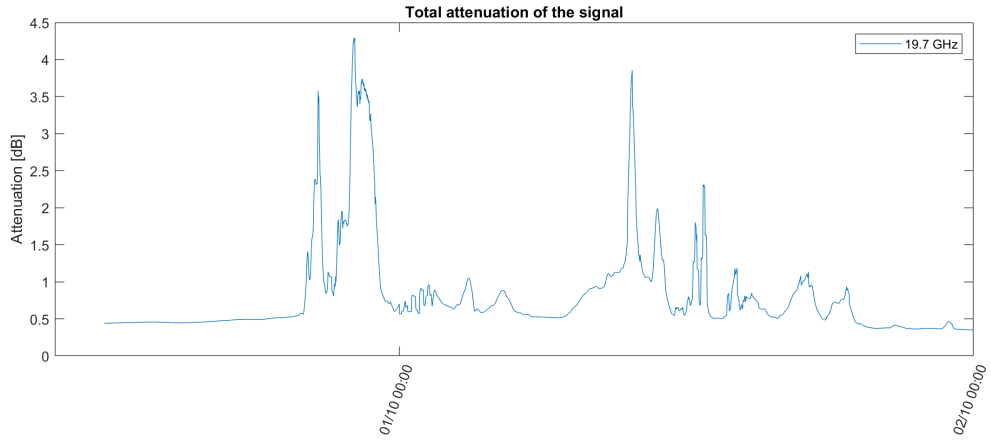

Figure 30: Total tropospheric attenuation prediction at 19.7 GHz

The tropospheric attenuation is frequency dependent. Figure 31 compares the total attenuation at 19.7 GHz and 39.4 GHz. The dependence of attenuation on frequency is visible; the higher the frequency, the higher the attenuation.

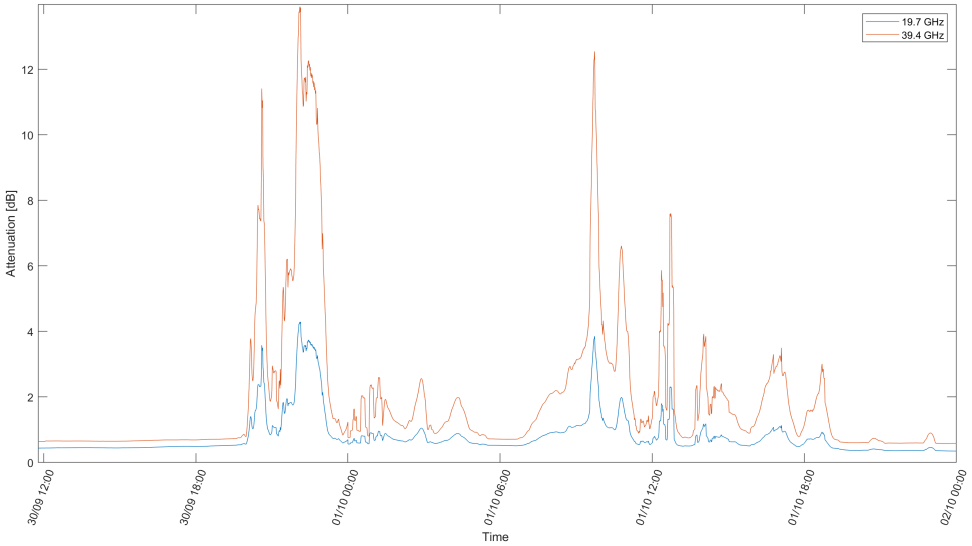

Figure 31: Total attenuation at 19.7 GHz and 39.4 GHz

6.1.1 Attenuation components

As discussed in section 2, the total tropospheric attenuation is the sum of four different components. Figures 32 and 33 show the attenuation level due to rain, fog and cloud, oxygen and water vapour at different frequencies. The gaseous attenuation depends on the meteorological conditions, but it can be noticed that the variations of the gaseous components are very low compared to the other contributions. Thus, when designing a telecommunication link, the gaseous contribution is always present. On the other hand attenuation due to rain, clouds and fog are intense events undergoing very strong variations in time. Thus the power required to guarantee the signal to noise ratio at the receiver is higher, if all meteorological conditions are considered. Since the attenuation due to rain is positively correlated to the rain rate, thus their distribution in time are similar.

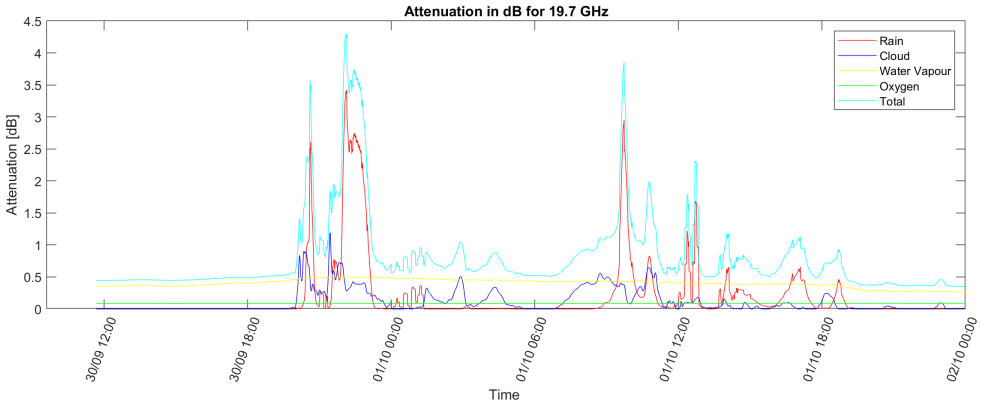

Figure 32: Attenuation components in dB at 19.7GHz

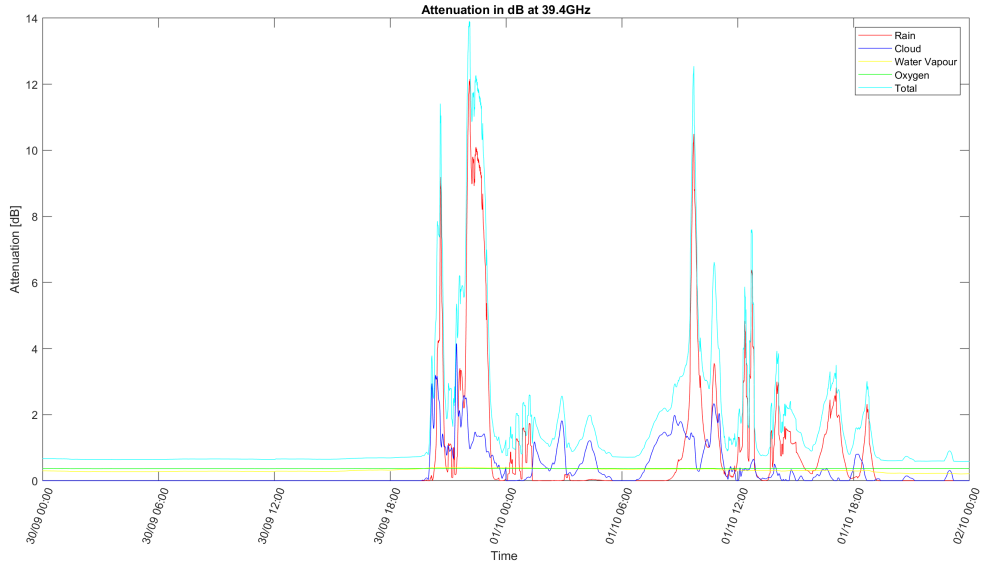

Figure 33: Attenuation components in dB at 39.4GHz

Figure 34, 35 and 36 present the specific attenuation intensity related to the different components for different heights.

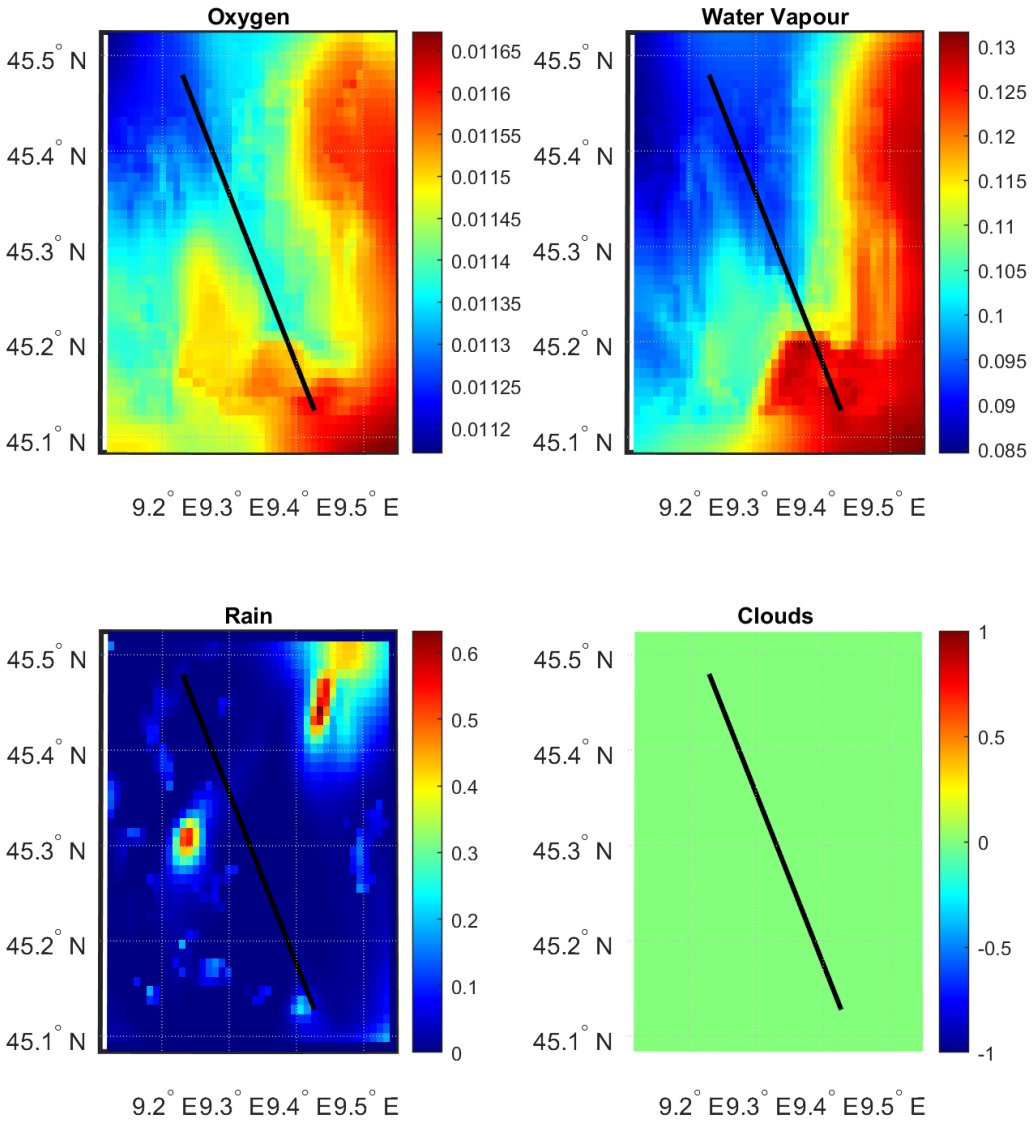

Figure 34: Specific attenuation amplitude at ground level for the 01/10/2018 at 13:20 and at 19.7 GHz

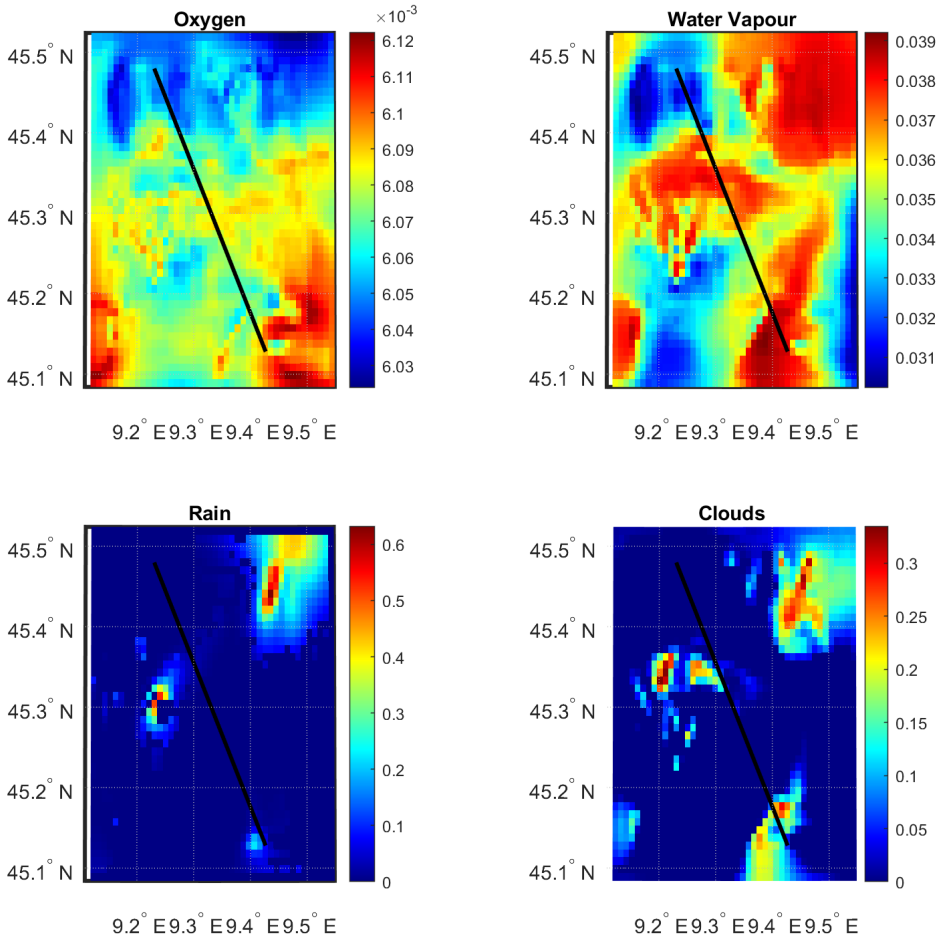

Figure 35: Specific attenuation amplitude at 3366m height for the 01/10/2018 at 13:20 and at 19.7 GHz

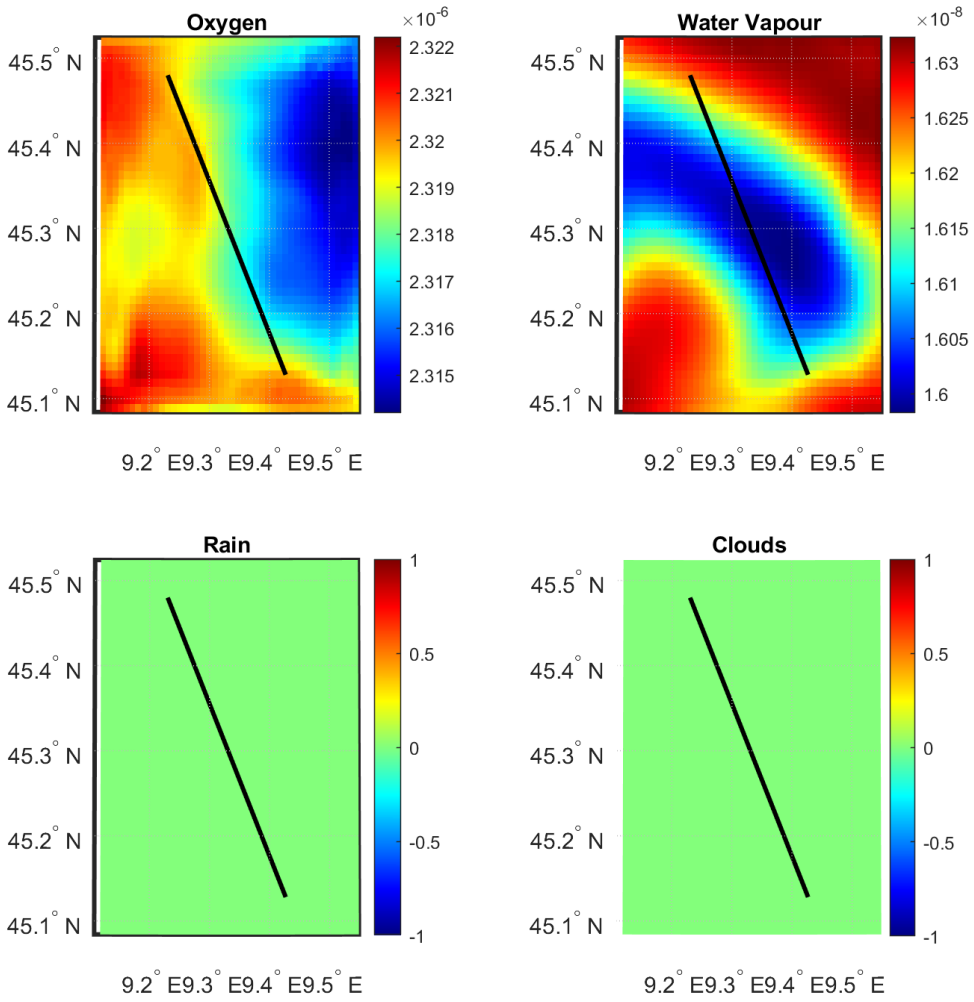

Figure 36: Specific attenuation amplitude at 30743m height for the 01/10/2018 at 13:20 and at 19.7 GHz

As seen in figures 34, 35, and 36, a strong difference in the variation rate of the attenuation is observable between the gaseous attenuation and the rain attenuation. While the gaseous attenuation undergoes small and smooth variations in space, the rain attenuation is very localized and matches the rain rate map presented in figure 29.

In figure 34 it can be noted that clouds are not producing any attenuation at ground level as expected without fog. The altitude in figure 35 is set to 3366m, which lies in a common range of altitude values for middle level clouds in temperate region [12]. Thus the cloud attenuation is not equal to zero. Finally figure 36 represents the attenuation at an altitude of 30743m. At this altitude all the components of the tropospheric attenuation reach negligible values compared to the level of attenuation in figures 34 and 35. In particular the attenuation due to rain, fog and cloud are equal to zero while the amplitude of the gaseous attenuation decreases by a factor 10^4 for the oxygen and 10^7 for the water vapour.

Figure 37 presents the specific attenuation of the different components as a function of the altitude.

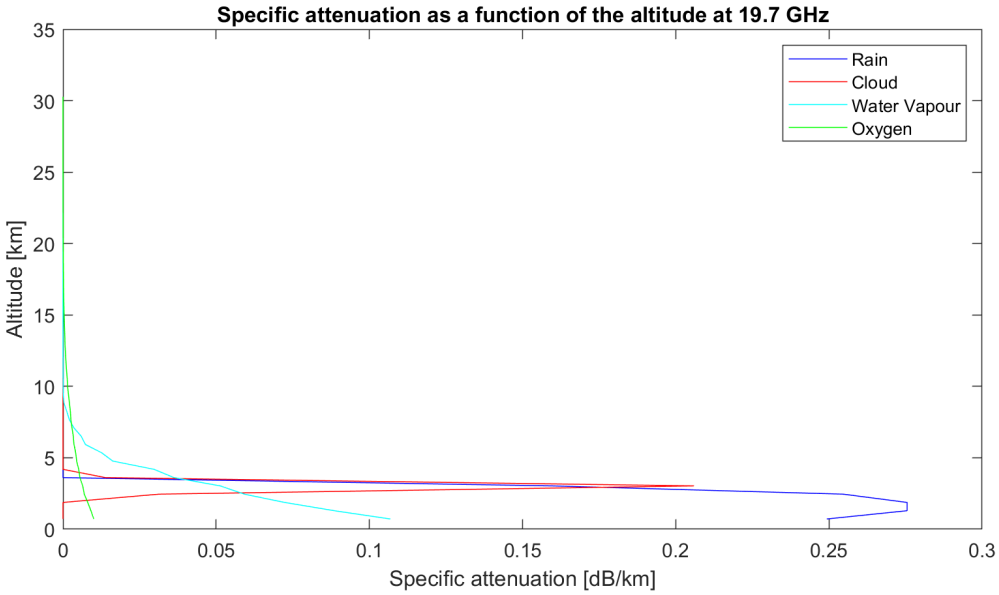

Figure 37: Specific attenuation as a function of the altitude for the 30/09/2018 at 22:59pm at of 19.7 GHz

Figure 38 presents the superposition of the attenuation for every minutes for the whole simulation period. The gaseous attenuation decreases exponentially with the altitude while the attenuation due to rain and clouds are bounded below 2 km height for these specific events. These results validate the assumption that the attenuation due to oxygen and water vapour is negligible above 30 km height. The attenuation due to rain and clouds is limited in altitude by the altitude of the clouds. The altitudes of the clouds are limited to 8km in polar regions and 18km in tropical regions[12].

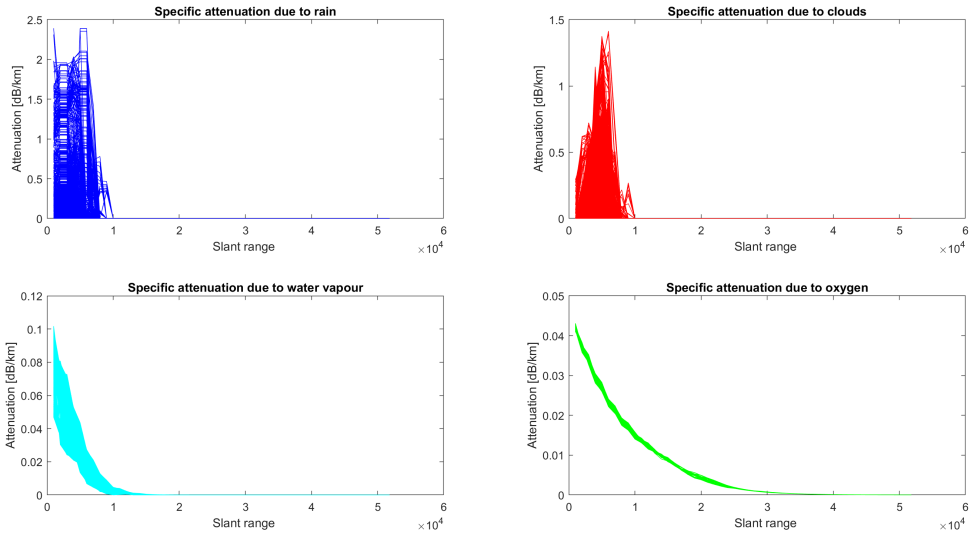

Figure 38: Superposition of the attenuation for every minute for the whole simulation period

6.1.2 Variation in the Ground station position

Given the limited accuracy of NWP models, this section explores how combining the information coming from different positions around the ground station might help increasing the significance of the attenuation predictions achieved using WRF. This is obtained by considering different pixels around the ground station. As presented in figure 39 the ground station is moved in a square of 11km centered around its real position. Given the long distance between the ground station and the spacecraft with respect to the variations in the ground station position. The elevation and azimuth angles can be considered as unchanged.

For simplicity the space variation dX is taken equal to the size of one pixel. Thus shifting the ground station of $k \cdot dX$ is equivalent to shifting the link of k pixels.

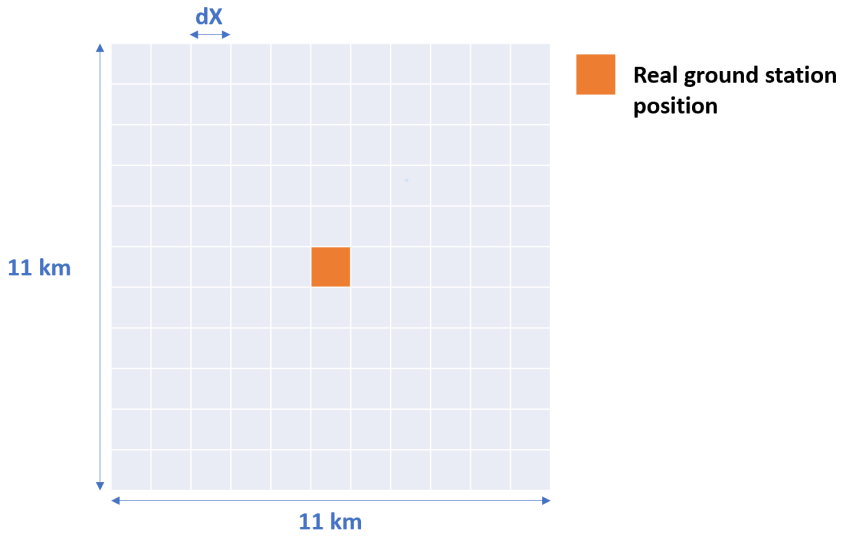

Figure 39: Variations in the ground station position

The results are plotted in figures 40 and 41. The set of attenuation values obtained from the variation in the ground station position are gathered for every time step. This leads to a set of 121 value for the attenuation for every time step. Then several statistical parameters are derived for each set a values :

- the median value
- the maximum and minimum values
- the values exceeded for 25% and 75% of the samples

The minimum to maximum interval, reported as "Max-Min interval" in the figures, represents the envelope of all the values of the attenuation derived for the period. The total attenuation computed with the real position of the ground station is also plotted with a gray line.

For the 30/09/2018, in figure 40, the atmospheric conditions can be considered as clear sky until 18:49. Thus during this period of time, the attenuation is due to the presence of oxygen and

water vapour as it can be seen in figure 30. It can be noticed that both intervals are extremely narrow, meaning that a variation of 5km in the ground station position does not imply a strong variation in the resulting total attenuation. A zoom in this period is presented in figure 42. The higher variation represents only a relative change of 6.19%. However after 18:49, when the rain event occurs, the intervals increase considerably. Indeed the Max- Min interval ranges from almost a clear sky attenuation level up to more than 3 times the maximum attenuation predicted with the real position of the ground station, leading to a relative difference of 785% at 20:47. Very similar conclusions can be drawn from the results for the second day in figure 41. It means that the computation of the attenuation during rain events is very sensitive to the position of the ground station. It is obvious that rain events represent the main challenge for the prediction. In the light of this result, it is more realistic to rely on a statistical approach for the operation of the link, which is intended to reduce the uncertainties coming from the high spatial variability of the predictions obtained with WRF.

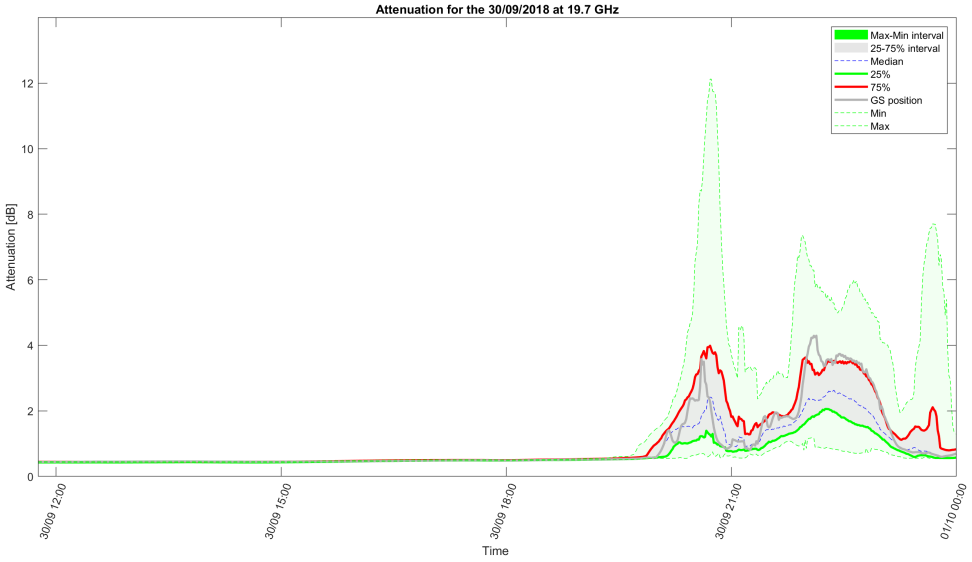

Figure 40: Total attenuation with variations in the ground station position at 19.7GHz for the 30/09/2018

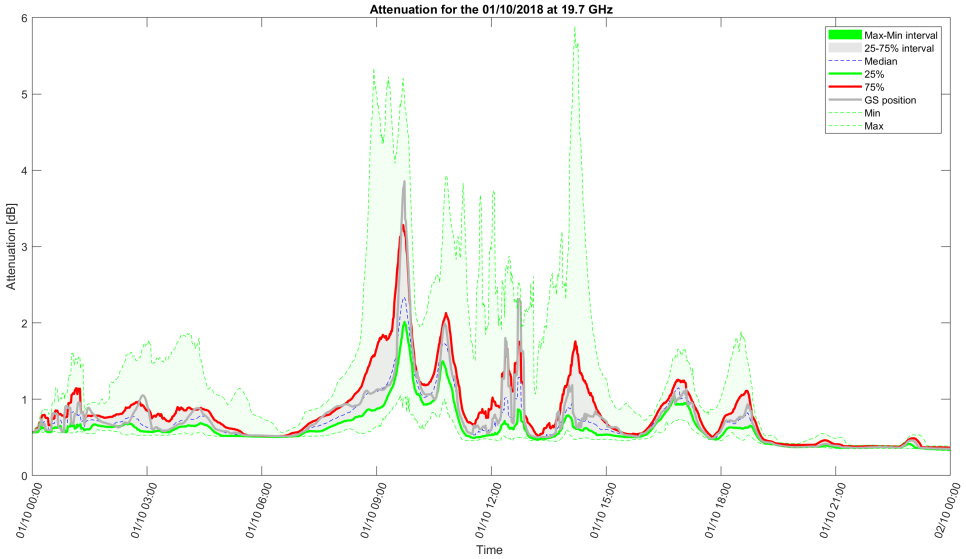

Figure 41: Total attenuation with variations in the ground station position at 19.7GHz for the 01/10/2018

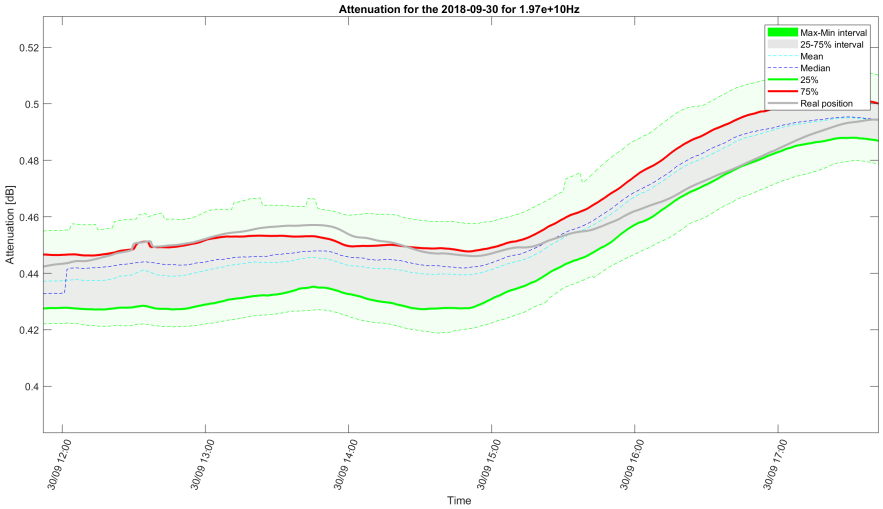

Figure 42: Interval of values outside rain events at 19.7GHz

6.1.3 Validation of the model from real data

Figures 43 and 44 present a comparison between the attenuation predicted from the WRF simulation and the attenuation measured with the experimental set-up presented in section 5.1. It can be noted that while the rain events are globally well identified, the WFR prediction seems to "anticipate" the measurement for the 30/09/2018 and to "delay" it for the 01/10/2018. However, outside rain events, the attenuation computed from WRF fits well the real attenuation represented by the black line. In figure 45, a zoom on the clear sky period is plotted. The relative difference between the prediction and the measurement is in the order of 10% and thus is a relatively good prediction of the attenuation. The shifting in time of the attenuation leads to a low reliability of the prediction in time. Thus a statistical approach is preferred to evaluate the risk of exceeding a certain value of attenuation. This statistical approach is presented in section 6.1.4.

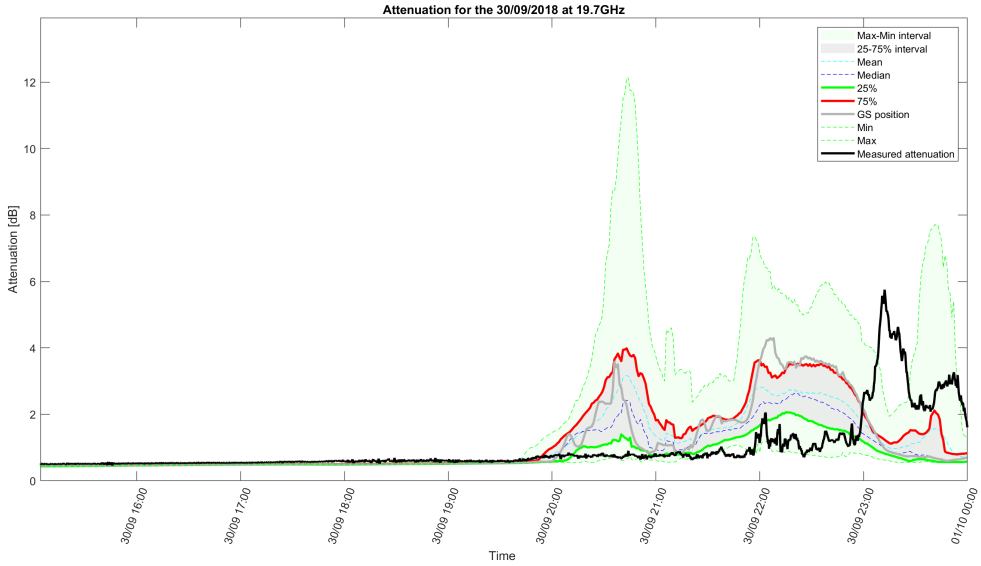

Figure 43: Comparison between the simulation prediction and the attenuation measured for the 30/09/2018 at 19.7 GHz

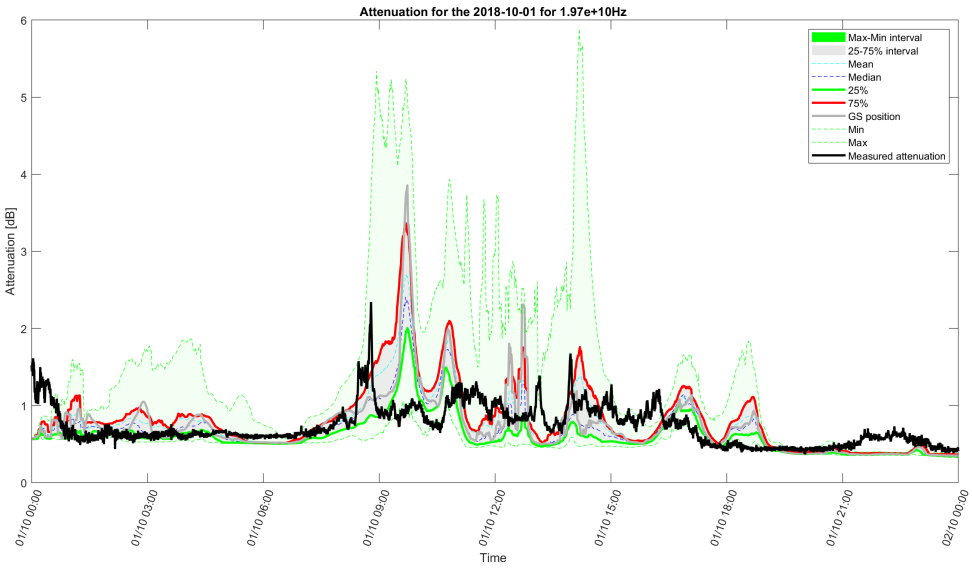

Figure 44: Comparison between the simulation prediction and the attenuation measured for the 30/09/2018 at 19.7 GHz

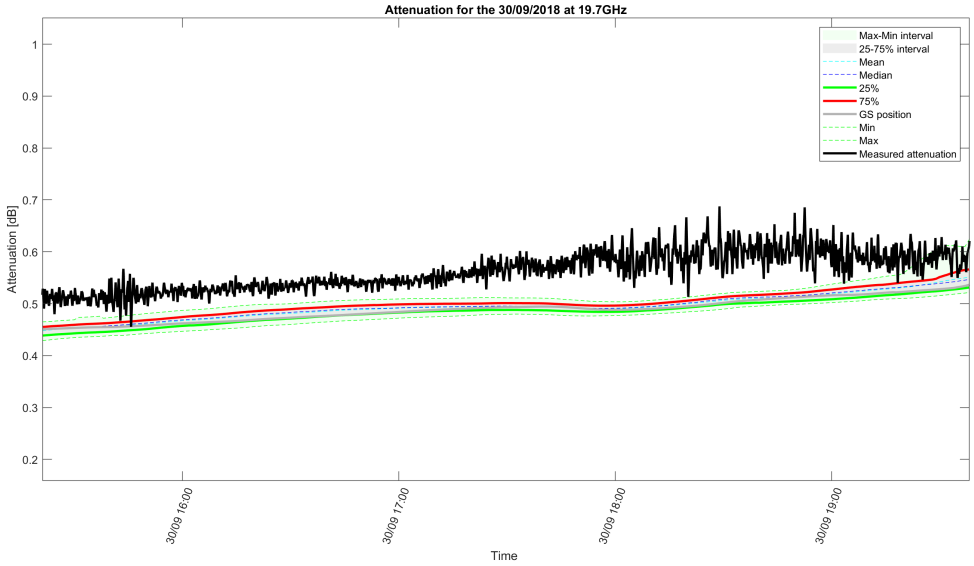

Figure 45: Comparison between the simulation prediction and the attenuation measured for the 01/10/2018 at 19.7 GHz - clear sky

6.1.4 Statistical analysis

The collection of WRF-based attenuation predictions or at least a full year would allow deriving the Complementary Cumulative Distribution Function of the attenuation (CCDF), which, in turn, could be used to design the trospopheric margin for a given system availability. This aspect is not explored in this work, due to the long computation times required by WRF. Indeed, the results obtained in this work are intended to explore the use of WRF-based predictions for the operation of an Earth-space link, whose features (e.g. transmit power and/or modulation and coding scheme) can be adapted in time as a function of the predicted attenuation. In order to implement such an approach, the statistical analysis is performed every 3 hours. All the attenuation levels computed are gathered from time $t - 90$ *minutes* to $t + 90$ *minutes* and for all the variations in the ground station position. Then the complementary cumulative distribution function (CCDF) is computed. Figures 46, 47, 48 and 49 present the CCDFs for the 3-hour slots of the simulation period. Thus, every CCDF can be used to identify the power margin to guaratee the correct operaton of the link in the associated time slot, i.e. to meet the target availability time; on the other hand, fixing the tropospheric margin, the CCDFs provide information on the expected risk of link outage: this is shown, as an example, in Figure 50.

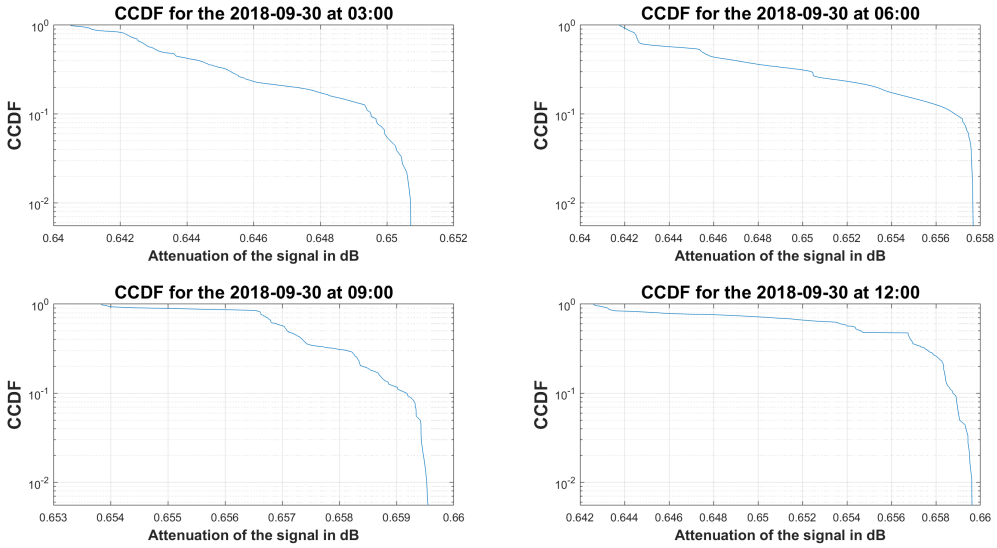

Figure 46: Complementary cumulative distribution function at 39.4 GHz - 30/09/2020 from 3:00 to 12:00

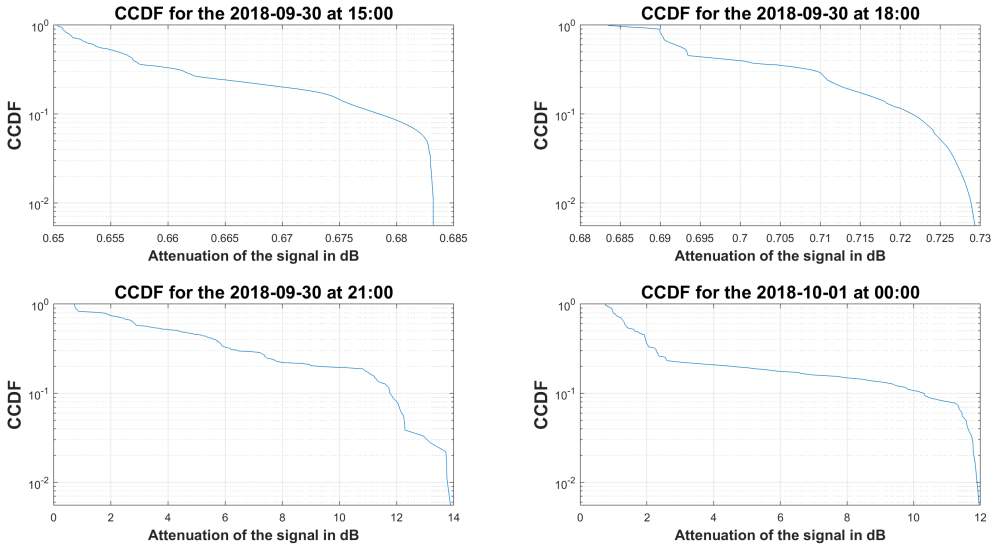

Figure 47: Complementary cumulative distribution function at 39.4 GHz - from the 30/09/2020 at 15:00 to the 01/10/2020 at 00:00

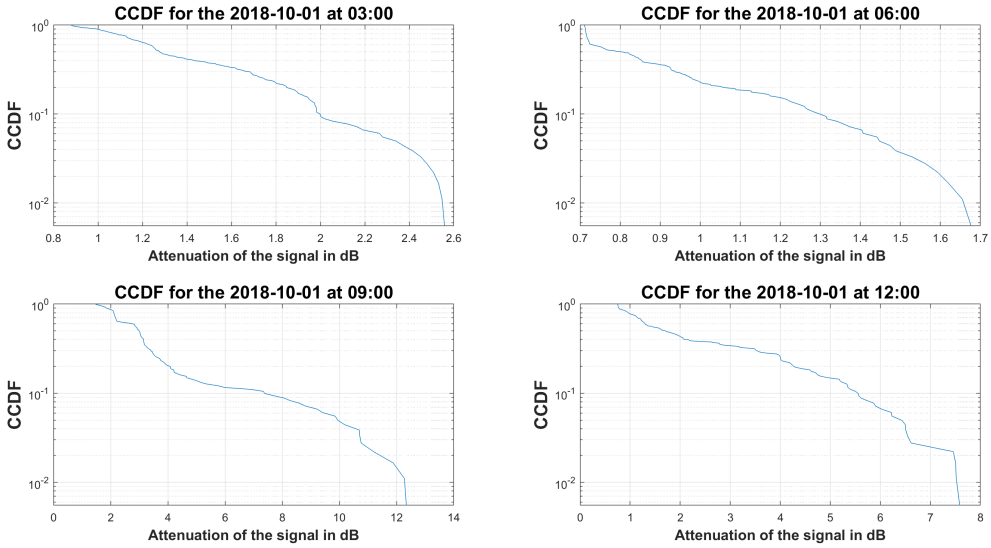

Figure 48: Complementary cumulative distribution function at 39.4 GHz - 01/10/2020 from 3:00 to 12:00

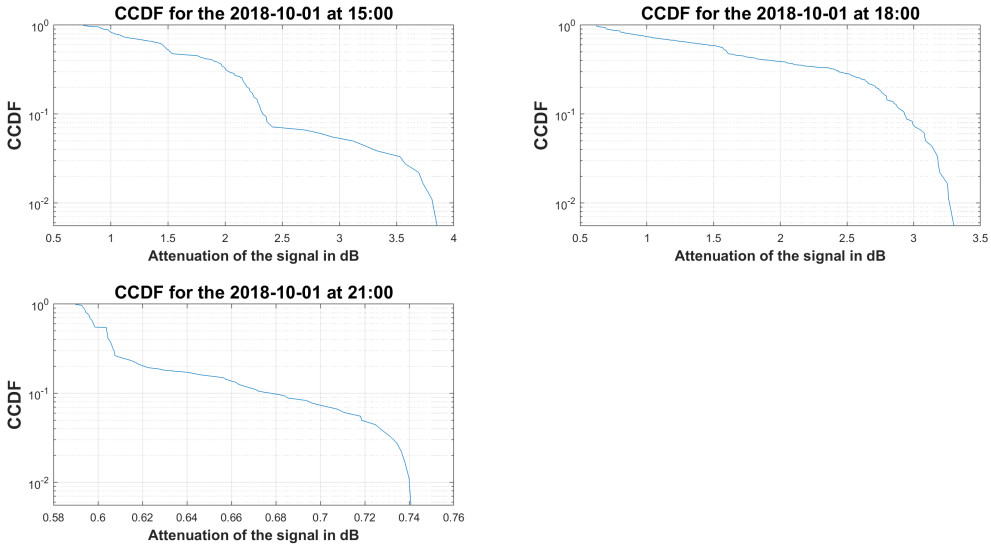

Figure 49: Complementary cumulative distribution function at 39.4 GHz - from the 01/10/2020 at 15:00 to the 02/10/2020 at 00:00

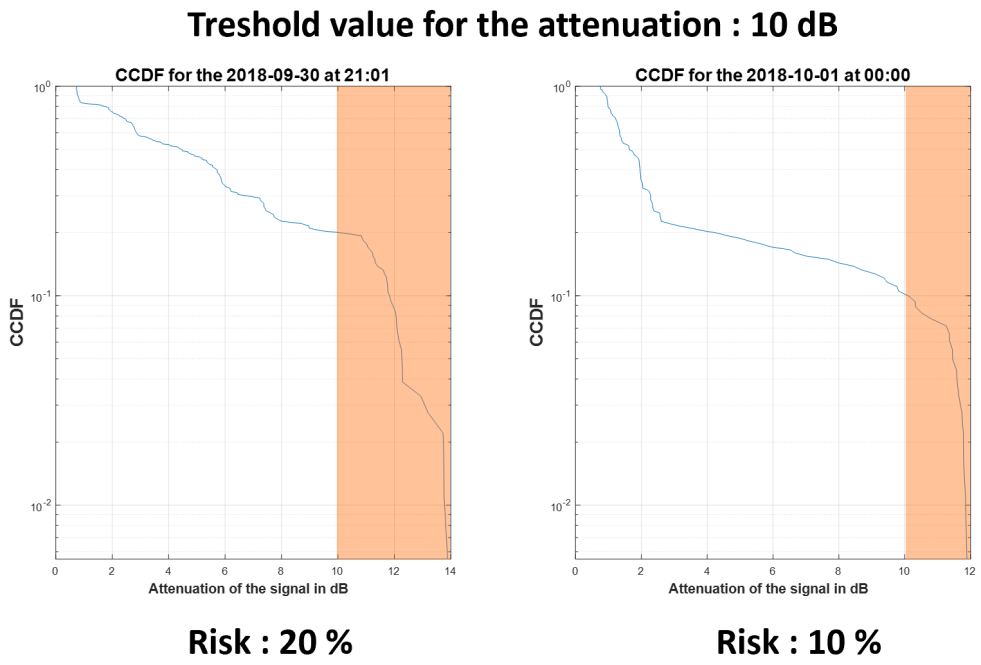

Figure 50: Example of interruption risk evaluation

6.2 Impact of time resolution

The time step is an important parameter since it affects both the accuracy of the results and the computational time. The choice of the time step should result from a trade off consideration between these two objectives. In this subsection, the results for different values of the time step are presented in figure 51. The variations of the time step are not affecting the integration scheme of the WRF simulation. Indeed the integration time is constrained by the space resolution, verifying equation 20. Thus the difference lies in the written frequency of the data inside the WRF output files. This has an impact both on the execution time of the WRF simulation and on the size of the output files, but also on the post processing time. However increasing too much the time step introduces an approximation error due to the interpolation of the attenuation. In this subsection a simple linear interpolation scheme is used. According to ITU, a time step of 1 minute for the rain rate evaluation is recommended if available [13]. From figure 51, it can be noted that the increase in the time step gives a good approximation up to a time step of 5 minutes. Beyond, the approximations induced become significant. On the other hand decreasing the time step down to 30 seconds does not provide a better prediction. In figure 52, when the rain event is really sudden and intense, the approximation becomes significant for a time step of 5 minutes and higher. Thus using a time step between 1 and 5 minutes seems to be a good compromise.

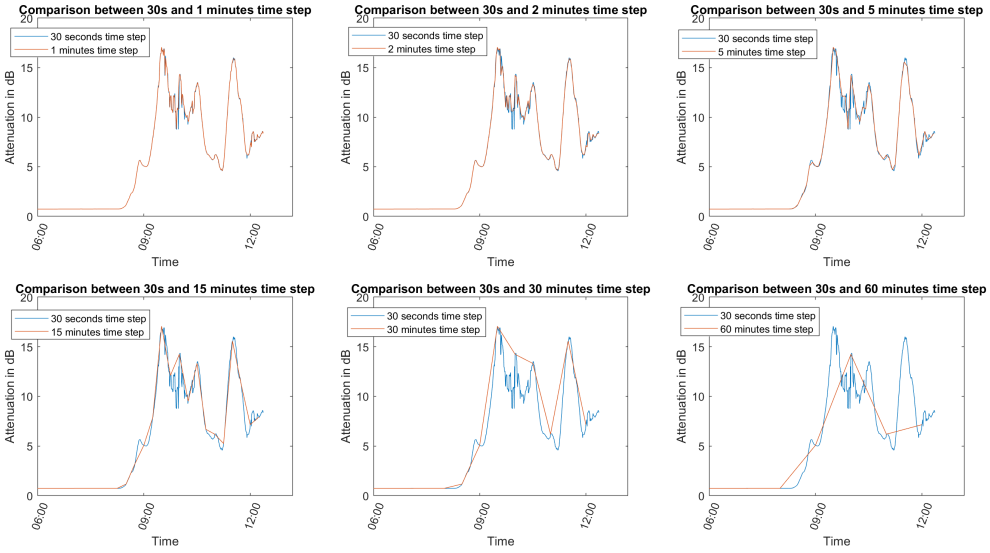

Figure 51: Comparison of the attenuation for different time step for the 01/10/2018 at 39.4 GHz

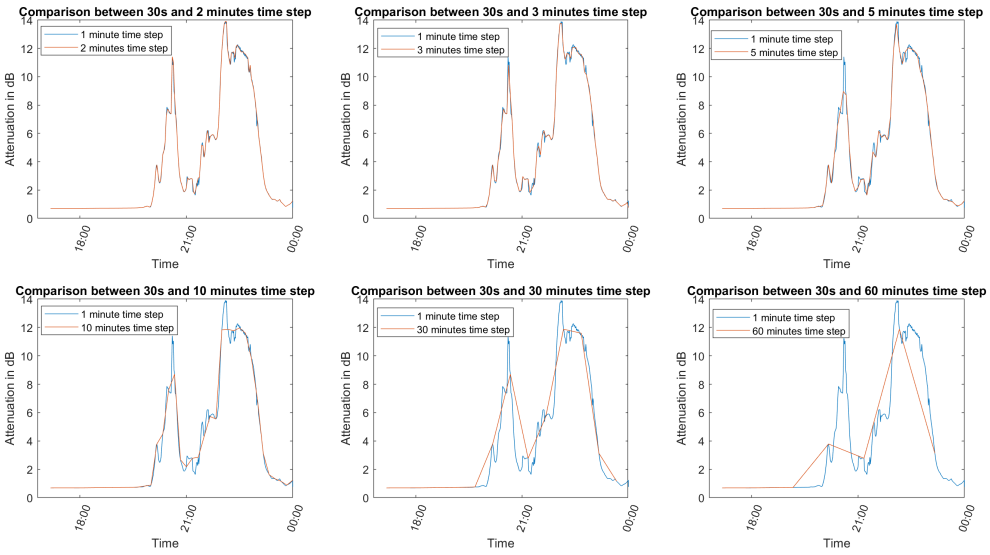

Figure 52: Comparison of the attenuation for different time step for the 30/09/2018 at 39.4 GHz

However, the comparison performed in this section can be used only for evaluating the sampling frequency required to capture the meteorological events. Thus for a proper evaluation of the attenuation the rain rate should be computed again by differentiating the total accumulated rain by the new time steps.

6.3 Impact of space resolution

During the WRF simulation the grid resolution is improved 2 times, going from $\simeq$ 27km resolution down to $\simeq$ 5km resolution and finally to $\simeq$ 1km resolution. This subsection draws a comparison between the 5km grid and the 1km grid for the same time step of 1 minute. The

attenuation, the attenuation error and the relative error are plotted in figure 53. The increase in the grid cell size does not allow capturing the sudden spatial variations of the attenuation. The attenuation curve is consequently smoother. For this particular simulation, the relative error increases up to 120 % and the difference reaches more than 5dB.

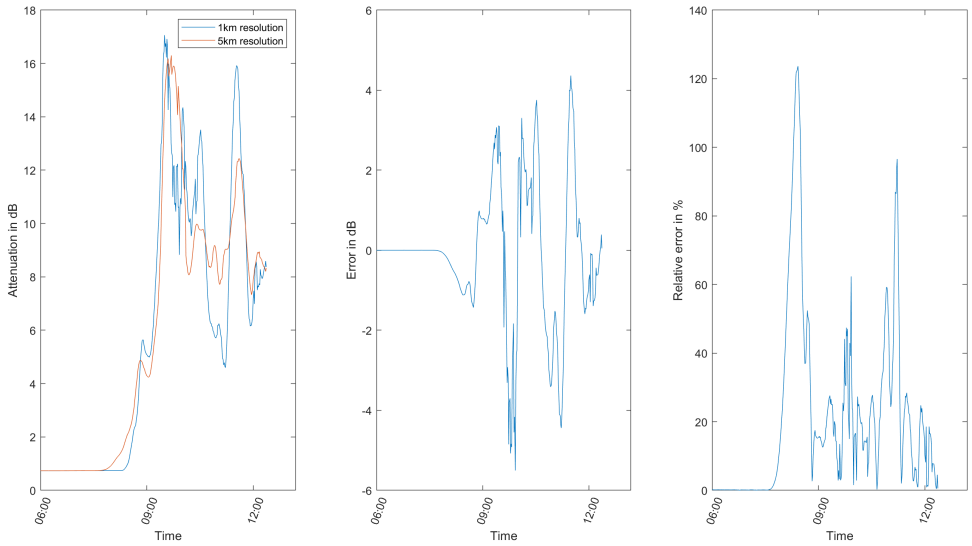

Figure 53: Comparison between the 5km and 1km grid for the 01/10/2018 at 39.4 GHz

6.4 Optimal computational time

This section presents the results obtained without improving the ERA5 grid resolution. The output data from WRF have been generated with a grid resolution of 0.25° ($\simeq$ 27 km) and a time step of 2 minutes and 30 seconds. The value of the time step is chosen to verify equation 20. Consequently this case corresponds to the fastest computation option using WRF. The slant path of the link crosses only 3 pixels, respectively 1 pixel for the longitude and 3 pixels for the latitude. The results are plotted in figures 54 and 55. The data are compared with the high resolution simulation that corresponds to the basic configuration of this thesis : 1km for the grid resolution and 1 minute for the time step. The attenuation due to gases are similar in both cases. However the total attenuation computed with the low resolution data is considerably smoothed over time. Indeed the poor discretization in space cannot capture the space distribution of rain and clouds. Some rain events do not appear for the low resolution (e.g. at 17:00). Inversely the cloud coverage influence is considerably overestimated for the low resolution data compared to the high resolution case.

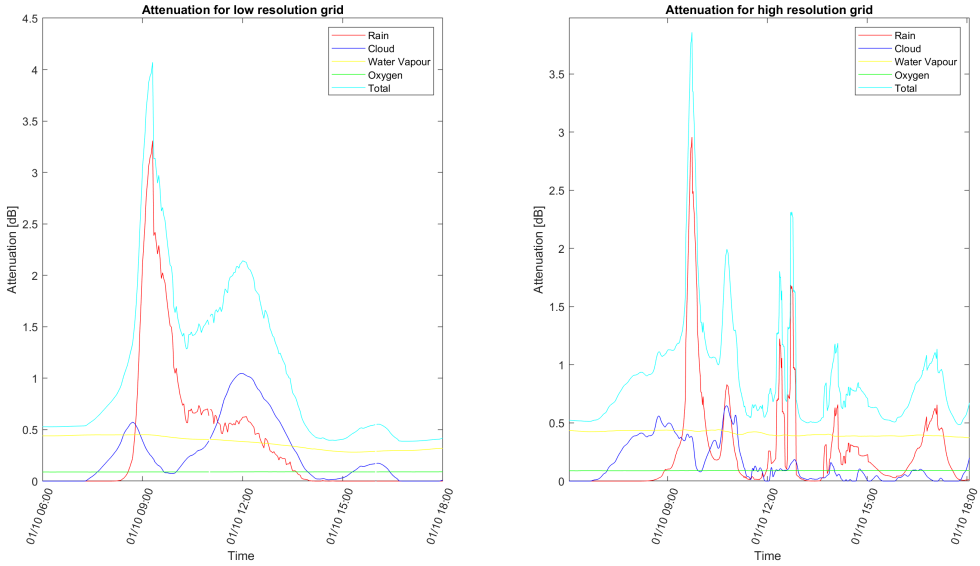

Figure 54: Comparison between low (left) and high (right side) resolution for the meteorological data at 19.7GHz

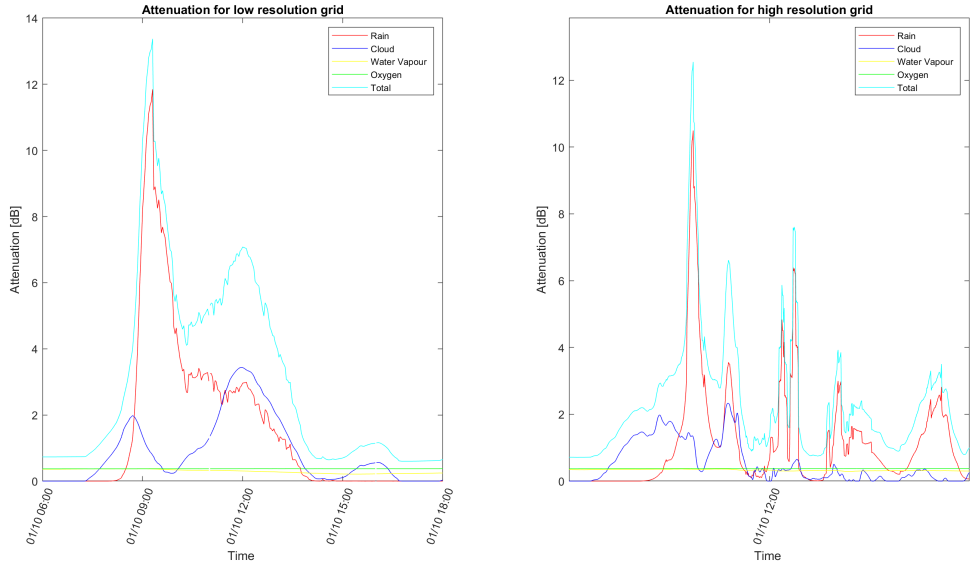

Figure 55: Comparison between low (left) and high (right side) resolution for the meteorological data at 39.4GHz

7 Conclusions and future work

The study conducted in this thesis has led to the generation of high resolution meteorological forecasts, down to 1km of grid resolution and down to 30 seconds in time. These data have been used for the prediction of the tropospheric attenuation for high frequency Earth-space links. In the light of the results presented in section 6, the following conclusions can be drawn :

- the time discretization used for the WRF simulation can be kept between 1 and 5 minutes. Using a smaller time step does not provide a significant improvement in the accuracy. A 1 minute time step is able to capture the sudden variations related to rain, clouds, and gases. On the other hand using a time step longer than 5 minutes should be discouraged since it does not allow to capture the variations of the meteorological variables previously mentioned.

- using a spatial grid of 1km improves the level of detail for the attenuation prediction compared to a 5km grid resolution

- the prediction of the attenuation using the WRF simulation provides reliable results for clear sky conditions. It means that the attenuation due to oxygen and water vapour are well predicted. However, regarding the attenuation due to clouds and rain, the simulation does not provide very reliable predictions. The level of attenuation expected is in the right order of magnitude if compared to the measured attenuation. However the attenuation peaks due to the rain events from the WRF predictions and the measurements hardly match in time. Thus, the direct exploitation of the predictions as a function of time is not reliable for identifying precisely the level of attenuation undergone by the link. However a statistical analysis can provide a more reliable basis to evaluate the risk of link outage over a longer time period, e.g. 1 or 3 hours.

- the attenuation levels for rain events computed with WRF are highly sensitive to the ground station position : a shift of some kilometers can lead to strong variations in the attenuation levels. On the other hand, the attenuation due to gases and clouds component present a relatively low sensitivity to the ground station position.

Here are some development paths that would be worthwhile being further explored in future works:

- investigate a longer period of time, in order to better validate the results obtained in this thesis and further analyze what are the factors influencing the most the accuracy in the predictions; moreover, simulations covering at least a year would allow assessing the usability of the prediction approach proposed in this work for the design of Earth-space links.

- identify a trade off analysis between the resolution of the meteorological data from WRF and the computational time required for the generation of high resolution data and their post processing

- compare the outputs obtained by using the ERA5 pressure and model levels as input to WRF

- further tests can corroborate the approach based on the short-period CCDFs of the attenuation for the adaptive operation of Earth-space links

Reference documents

[1] *ITU-R P.676-10 recommendation*. ITU. URL: https://www.itu.int/dms_pubrec/itu-r/rec/p/R-REC-P.676-10-201309-S!!PDF-E.pdf.

[2] *ITU-R P.838-3 recommendation*. ITU. URL: https://www.itu.int/dms_pubrec/itu-r/rec/p/R-REC-P.838-3-200503-I!!PDF-E.pdf.

[3] *ITU-R P.840-8 recommendation*. ITU. URL: https://www.itu.int/dms_pubrec/itu-r/rec/p/R-REC-P.840-8-201908-I!!PDF-E.pdf.

[4] *MODELING SYSTEM OVERVIEW*. WRF User Page. URL: https://www2.mmm.ucar.edu/wrf/users/model.html.

[5] *WRF Online Tutorial*. WRF User Page. URL: https://www2.mmm.ucar.edu/wrf/OnLineTutorial/index.php.

[6] *ARW-Version 4 Modeling System User's Guide*. Mesoscale, Microscale Meteorology Laboratory, and National Center for Atmospheric Research. Jan. 2019. URL: https://www2.mmm.ucar.edu/wrf/users/docs/user_guide_v4/contents.html.

[7] *A Matlab toolbox for working with common data model datasets*. NCTOOLBOX. URL: https://nctoolbox.github.io/nctoolbox/.

[8] *Available GRIB Datasets from NCAR*. WRF User Page. URL: https://www2.mmm.ucar.edu/wrf/users/download/free_data.html.

[9] *Download of the CDS API package*. The Python Package Index. URL: https://pypi.org/project/cdsapi/.

[10] *namelist.wps: Best Practices*. WRF User Page. URL: https://www2.mmm.ucar.edu/wrf/users/namelist_best_prac_wps.html.

[11] *ITU-R P.618-13 recommendation*. ITU. URL: https://www.itu.int/dms_pubrec/itu-r/rec/p/R-REC-P.618-13-201712-I!!PDF-E.pdf.

[12] *Definitions, International Cloud Atlas*. World Meteorological Organization. Mar. 2017. URL: https://cloudatlas.wmo.int/en/clouds-definitions.html.

[13] *ITU-R P.837-7 recommendation*. ITU. URL: https://www.itu.int/dms_pubrec/itu-r/rec/p/R-REC-P.837-7-201706-I!!PDF-E.pdf.